

1 **Image-based surface reconstruction in geomorphometry –** 2 **merits, limits and developments**

3

4 **A. Eltner¹, A. Kaiser², C. Castillo³, G. Rock⁴, F. Neugirg⁵ and A. Abellan⁶**

5 [1] {Institute of Photogrammetry and Remote Sensing, Technical University Dresden,
6 Germany}

7 [2] {Soil and Water Conservation Unit, Technical University Freiberg, Germany}

8 [3] {Dep. of Rural Engineering, University of Córdoba, Spain}

9 [4] {Dep. of Environmental Remote Sensing and Geomatics, University of Trier, Germany}

10 [5] {Dep. of Physical Geography, Catholic University Eichstätt-Ingolstadt, Germany}

11 [6] {Risk Analysis Group, Institute of Earth Sciences, University of Lausanne, Switzerland}

12 Correspondence to: A. Eltner (Anette.Eltner@tu-dresden.de)

13

14 **Abstract**

15 Photogrammetry and geosciences have been closely linked since the late 19th century due to
16 the acquisition of high-quality 3D datasets of the environment, but it has so far been restricted
17 to a limited range of remote sensing specialists because of the considerable cost of metric
18 systems for the acquisition and treatment of airborne imagery; Nowadays, a wide range of
19 commercial and open-source software tools enable the generation of 3D and 4D models of
20 complex geomorphological features by geoscientists and other non-experts users. In addition,
21 very recent rapid developments in unmanned aerial vehicle (UAV) technology allows for the
22 flexible generation of high quality aerial surveying and orthophotography at a relatively low-
23 cost.

24 The increasing computing capabilities during the last decade, together with the development
25 of high-performance digital sensors and the important software innovations developed by
26 computer based vision and visual perception research fields have extended the rigorous
27 processing of stereoscopic image data to a 3D point cloud generation from a series of non-
28 calibrated images. Structure from motion (SfM) workflows are based upon algorithms for
29 efficient and automatic orientation of large image sets without further data acquisition
30 information, examples including robust feature detectors like the scale-invariant feature

31 transform for 2D-imagery. Nevertheless, the importance of carrying out well-established
32 fieldwork strategies, using proper camera settings, ground control points and ground truth for
33 understanding the different sources of errors still need to be adapted in the common scientific
34 practice.

35 This review intends not only to summarize the current state of the art on using SfM
36 workflows in geomorphometry, but also to give an overview of terms and fields of
37 application. Furthermore, this article aims to quantify already achieved accuracies and used
38 scales using different strategies, to evaluate possible stagnations of current developments and
39 to identify key future challenges. It is our belief that some lessons learned from
40 former articles, scientific reports and book chapters concerning the identification of common
41 errors or “bad practices” and some other valuable information may help in guiding the future
42 use of SfM photogrammetry in geosciences.

43

44 **1 Introduction**

45 Early works on projective geometries date back to more than five centuries, when scientists
46 derived coordinates of points from several images and investigated the geometry of
47 perspectives (Doyle, 1964). Projective geometry represents the basis for the developments in
48 photogrammetry in the late 19th century, when Aimé Laussedat experimented with terrestrial
49 imagery as well as kites and balloons for obtaining imagery for topographic mapping
50 (Laussedat, 1899). Rapidly, photogrammetry advanced to be an essential tool in geosciences
51 during the last two decades and is lately gaining momentum driven by digital sensors leading
52 to flexible, fast and facile generation of images. Simultaneously, growing computing
53 capacities and rapid developments in computer vision led to the method of Structure from
54 Motion (SfM) that opened the way for low-cost high-resolution topography. Thus, the
55 community using image-based 3D reconstruction experienced a considerable growth, not only
56 in quality and detail of the achieved results but also in the number of potential users from
57 diverse geo-scientific disciplines.

58 SfM photogrammetry can be performed with images acquired by consumer grade digital
59 cameras and is thus very flexible in its implementation. Its ease of use in regard to data
60 acquisition and processing makes it further interesting to non-experts (Fig. 1). The diversity of
61 possible applications led to a variety of terms used to describe SfM photogrammetry either
62 from a photogrammetric or a computer vision standpoint. Thus, to avoid ambiguous
63 terminology, a short list of definitions in regard to the reviewed method is given in Table 1. In

64 this review a series of studies that utilise the algorithmic advance of high automation in SfM
65 are considered, i.e. no initial estimates of the image network geometry or user interactions to
66 generate initial estimates are needed. Furthermore, data processing can be performed almost
67 fully automatically. However, some parameter settings, typical for photogrammetric tools
68 (e.g. camera calibration values), can be applied to optimise both accuracy and precision, and
69 GCP or scale identification are still necessary.

70 SfM photogrammetry can be applied to a vast range of temporal scales (reaching from sub-
71 seconds to decades) as well as spatial scales (reaching from sub-millimetres to kilometres)
72 and resolutions up to an unprecedented level of detail, allowing for new insights into earth
73 surface processes, i.e. 4D (three spatial dimensions and one temporal dimension)
74 reconstruction of environmental dynamics. For instance, the concept of sediment connectivity
75 (Bracken et al., 2014) can be approached from a new perspective through varying spatio-
76 temporal scales. Thereby, the magnitude and frequency of events and their interaction can
77 also be evaluated. Furthermore, the versatility of SfM photogrammetry utilising images
78 captured from aerial or terrestrial perspectives has the advantage of being applicable in remote
79 areas with limited access and in fragile, fast changing environments.

80 After the suitability of SfM has been noticed for geo-scientific applications (James and
81 Robson, 2012, Westoby et al., 2012, Fonstad et al., 2013) the number of studies utilising SfM
82 photogrammetry for geomorphometric investigations (thereby referring to the “science of
83 topographic quantification” based on Pike et al., 2008) has increased significantly. However,
84 the method needs a sophisticated study design and some experience in image acquisition to
85 prevent predictable errors and to ensure good quality of the reconstructed scene. Smith et al.
86 (2015) and Micheletti et al. (2015) recommend a setup for efficient data acquisition.

87 A total of 65 publications are reviewed in this study. They are chosen according to the
88 respective field of research and methodology. Only those studies that make use of the benefits
89 of automatic image matching algorithms, and thus apply the various SfM tools, are included.
90 Studies that lack of full automation are excluded, i.e. some traditional photogrammetric
91 software. Topic wise a line is drawn in regard to the term geosciences. The largest fraction of
92 the reviewed articles tackles questions arising in geomorphological contexts. To account for
93 the versatility of SfM photogrammetry, a few studies deal with plant growth on different
94 scales (moss, crops, forest) or investigate rather exotic topics such as stalagmites or reef
95 morphology.

96 This review aims to highlight the development of SfM photogrammetry as a valuable tool for
97 geoscientists:

98 (1) The method of SfM photogrammetry is briefly summarised and algorithmic differences
99 due to their emergence from computer vision as well as photogrammetry are clarified
100 (section 2).

101 (2) Open-source tools regarding SfM photogrammetry are introduced as well as beneficial
102 tools for data post-processing (section 3).

103 (3) Different fields of applications where SfM photogrammetry led to new perceptions in
104 geomorphometry are displayed (section 4).

105 (4) The performance of the reviewed method is evaluated (section 5).

106 (5) Frontiers and significance of SfM photogrammetry are discussed (section 6).

107

108 **2 SfM photogrammetry: method outline**

109 **2.1 Basic concept**

110 Reconstruction of three-dimensional geometries from images has played an important role in
111 the past centuries (Ducher, 1987, Collier, 2002). The production of high-resolution DEMs
112 was and still is one of the main applications of (digital) photogrammetry. Software and
113 hardware developments as well as the increase in computing power in the 1990s and early
114 2000s made aerial photogrammetric processing of large image datasets accessible to a wider
115 community (e.g. Chandler, 1999).

116 Camera orientations and positions, which are usually unknown during image acquisition, have
117 to be reconstructed to model a 3D scene. For that purpose, photogrammetry has developed
118 bundle adjustment (BA) techniques, which allow for simultaneous determination of camera
119 orientation and position parameters as well as 3D object point coordinates for a large number
120 of images (e.g. Triggs et al, 2000). BA needs image coordinates of many tie points as input
121 data. If the BA is extended by a simultaneous calibration option, even the intrinsic camera
122 parameters can be determined in addition to the extrinsic parameters. Furthermore, a series of
123 ground control points can be used as input into BA for geo-referencing the image block (e.g.
124 Luhmann et al., 2014, Kraus, 2007, Mikhail et al., 2001).

125 Parallel developments in computer vision took place that try to reconstruct viewing
126 geometries of image datasets not fulfilling the common prerequisites from digital
127 photogrammetry, i.e. calibrated cameras and initial estimates of the image acquisition scheme.

128 This led to the SfM technique (Ullman, 1979) allowing to process large datasets and to use a
129 combination of multiple non-metric cameras.

130 The typical workflow of SfM photogrammetry (e.g. Snavely et al., 2008) comprises the
131 following steps:

- 132 (1) identification and matching of homologous image points in overlapping photos (image
133 matching, e.g. Lowe, 1999),
- 134 (2) reconstruction of the geometric image acquisition configuration and of the corresponding
135 3D coordinates of matched image points (sparse point cloud) with iterative BA,
- 136 (3) dense matching of the sparse point cloud from reconstructed image network geometry,
- 137 (4) scaling or geo-referencing, which is also performable within step 2.

138 Smith et al. (2015) give a detailed description of the workflow of SfM photogrammetry,
139 especially regarding step 1 and step 2.

140 In contrast to classical photogrammetry software tools, SfM allows for reliable processing of
141 a large number of images in rather irregular image acquisition schemes (Snavely et al., 2008)
142 with a much higher degree of process automation. Thus, one of the main differences between
143 the usual photogrammetric workflow and SfM is the emphasis on either accuracy or
144 automation, with SfM focusing on the latter (Pierrot-Deseilligny and Clery, 2011). Another
145 deviation between both 3D reconstruction methods is the consideration of GCPs (James and
146 Robson, 2014, Eltner and Schneider, 2015). Photogrammetry performs BA either one-staged,
147 considering GCPs within the BA, or two-staged, performing geo-referencing after a relative
148 image network configuration has been estimated (Kraus, 2007). In contrast, SfM is solely
149 performed in the manner of a two-staged BA concentrating on the relative orientation in an
150 arbitrary coordinate system. Thus, absolute orientation has to be conducted separately with a
151 seven parameter 3D-Helmert-transformation, i.e. three shifts, three rotations and one scale.
152 This can be done, for instance, with the freeware tool `sfm-georef` that also gives accuracy
153 information (James and Robson, 2012). Using GCPs has been proven to be relevant for
154 specific geometric image network configurations, as parallel-axes image orientations usual for
155 UAV data, because adverse error propagation can occur due to unfavourable parameter
156 correlation, e.g. resulting in the non-linear error of a DEM dome (Wu, 2014, James and
157 Robson, 2014, Eltner and Schneider, 2015). Within a one-staged BA these errors are
158 minimised because additional information from GCPs is employed during the adjustment
159 calculation, which is not possible, when relative and absolute orientation are not conducted in
160 one stage.

161 The resulting oriented image block allows for a subsequent dense matching, measuring many
162 more surface points through spatial intersection to generate a DEM with very high resolution.
163 Recent developments in dense matching allow for resolving object coordinates for almost
164 every pixel. To estimate 3D coordinates, pixel values are either compared in image-space in
165 the case of stereo-matching, considering two images, or in the object space in the case of
166 MVS-matching, considering more than two images (Remondino et al., 2014). Furthermore,
167 local or global optimisation functions (Brown et al., 2003) are considered, e.g. to handle
168 ambiguities and occlusion effects between compared pixels (e.g. Pears et al., 2012). To
169 optimise pixel matching, (semi-)global constraints consider the entire image or image scan-
170 lines (e.g. semi-global matching (SGM) after Hirschmüller, 2011), whereas local constraints
171 consider a small area in direct vicinity of the pixel of interest (Remondino et al., 2014).

172 SfM photogrammetry software packages are available partially as freeware or even open-
173 source. Most of the packages comprise SfM techniques in order to derive 3D reconstructions
174 from any collection of unordered photographs, without the need of providing camera
175 calibration parameters and high accuracy ground control points. As a consequence, no in-
176 depth knowledge in photogrammetric image processing is required in order to reconstruct
177 geometries from overlapping image collections (James and Robson, 2012, Westoby et al.,
178 2012, Fonstad et al., 2013). But now, also many photogrammetric tools utilise abilities from
179 SfM to derive initial estimates automatically (i.e. automation) and then perform
180 photogrammetric BA with the possibility to set weights of parameters for accurate
181 reconstruction performance (i.e. accuracy). In this review studies are considered, which either
182 use straight SfM tools from computer vision or photogrammetric tools implementing SfM
183 algorithms that entail no need for initial estimates in any regard.

184

185 **2.2 Tools for SfM photogrammetry and data post processing**

186 SfM methodologies rely inherently on automated processing tools which can be provided by
187 different non-commercial or commercial software packages. Within the commercial approach,
188 PhotoScan (Agisoft LLC, Russia), Pix4D (Pix4D SA, Switzerland) and MENCİ APS
189 (MENCİ Software, Italy) represent complete solutions for 3D photogrammetric processing
190 that have been used in several of the reviewed works.

191 Initiatives based on non-commercial software have played a significant role in the
192 development of SfM photogrammetry approaches, either 1) open-source, meaning the source
193 code is available with a license for modification and distribution; 2) freely-available, meaning

194 the tool is free to use but no source code is provided or 3) under free web service with no
195 access to the code, intermediate results or possible secondary data usage (Table 2). The
196 pioneer works by Snavely et al. (2006, 2008) and Furukawa and Ponce (2010) as well as
197 Furukawa et al. (2010) provided the basis to implement one of the first open-source
198 workflows for free SfM photogrammetry combining Bundler and PMVS2/CMVS as in
199 SfMToolkit (Astre, 2015). By 2007, the MicMac project, which is open-source software
200 originally developed for aerial image matching, became available to the public and later
201 evolved to a comprehensive SfM photogrammetry pipeline with further tools such as APERO
202 to estimate image orientation (Pierrot-Deseilligny and Clery, 2011).

203 Further contributors put their efforts in offering freely-available solutions based on Graphical
204 User Interfaces (GUI) for SfM photogrammetry (VisualSfM by Wu, 2013) and geo-
205 referencing (sfm_georef by James and Robson, 2012). The need for editing large point-cloud
206 entities from 3D reconstruction led to the development of open-source specific tools such as
207 Meshlab (Cignoni et al., 2008) or CloudCompare (Girardeau-Montaut, 2015), also
208 implementing GUIs. Sf3M (Castillo et al., 2015) exploits VisualSfM and sfm_georef and
209 additional CloudCompare command-line capacities for image-based surface reconstruction
210 and subsequent point cloud editing within one GUI tool. Overall, non-commercial
211 applications have provided a wide range of SfM photogrammetry related solutions that are
212 constantly being improved on the basis of collaborative efforts. Commercial software
213 packages are not further displayed due to their usual lack of detailed information regarding
214 applied algorithms and their black box approach.

215 A variety of tools for SfM photogrammetry (at least 10 different) are used within the differing
216 studies of this review (Fig. 3). Agisoft PhotoScan is by far the most employed software,
217 which is probably due to its ease of use. However, this software is commercial and works on
218 the black box principle, which is in contrast to the second most popular tool Bundler in
219 combination with PMVS or CMVS. The tool APERO in combination with MicMac focuses
220 on accuracy instead of automation (Pierrot-Deseilligny and Clery, 2011), which is different to
221 the former two. The high degree of possible user-software interaction, which can be very
222 advantageous to adopt the 3D reconstruction to each specific case study, might also be its
223 drawback because further knowledge into the method is required. Only a few studies have
224 used the software in geo-scientific investigations (Bretar, et al., 2013, Stumpf et al., 2014,
225 Ouédraogo et al., 2014, Stöcker et al., 2015, Eltner and Schneider, 2015).

226

227 **3 Key developments in SfM photogrammetry**

228 The vast recognition of SfM photogrammetry resulted in a large variety of its implementation
229 leading to methodological developments, which have validity beyond its original application.
230 Thus, regarding geomorphometric investigations, studies considering field of applications as
231 well as evaluations of the method performance induced key advances for SfM
232 photogrammetry to establish as a standard tool in geosciences (Table 3). In the following, the
233 approach is introduced concerning the selection and retrieval of scientific papers utilising SfM
234 photogrammetry.

235 A survey of 65 scientific papers published between 2012 and 2015 was conducted, covering a
236 wide range of applications of SfM photogrammetry in geo-scientific analysis (see Appendix
237 A for a detailed list). Common scientific journals, academic databases and standard online
238 searches have been used to search for corresponding publications. Although, it has to be noted
239 that our approach does not guarantee full coverage of the published works using SfM
240 photogrammetry in geosciences. Nevertheless, various disciplines, locations and approaches
241 from all continents are contained in this review (Fig. 2).

242 To put research hot spots in perspective it should be taken into account that the amount of
243 publications in each discipline is not only dependent on the applicability of the method in that
244 specific field of research. To a greater degree it is closely linked to the overall number of
245 studies, which in the end can probably be broken down to the actual amount of researchers in
246 that branch of science. Relative figures revealing the relation between SfM photogrammetry
247 oriented studies to all studies of a given field of research would be desirable but are beyond
248 the scope of this review.

249

250 The previously described advantages of the method have introduced a new group of users,
251 leading to a variety of new studies in geomorphic surface reconstruction and analysis.
252 Different disciplines started to use SfM algorithms more or less simultaneously.

253 A list of all topics reviewed in this manuscript according to their year of appearance is shown
254 in Table 4. It is important to note that most subjects are not strictly separable from each other:
255 For instance, a heavy flash flood event will likely trigger heavy damage by soil erosion or
256 upstream slope failures. Thus, corresponding studies are arranged in regard to their major
257 focus. The topic soil science comprises studies of soil erosion as well as soil micro-
258 topography.

260 **3.1 Soil science**

261 An identification of convergent research topics of SfM photogrammetry in geosciences
262 revealed a distinct focus on erosional processes, especially in soil erosion (11 studies).
263 Gullies, as often unvegetated and morphologically complex features of soil erosion, are
264 predestined to serve as a research object (6 studies) to evaluate SfM performance. One of the
265 first works on SfM in geosciences from 2012 compared established 2D and 3D field methods
266 for assessing gully erosion (e.g. LiDAR, profile meter, total station) to SfM data with regard to
267 costs, accuracy and effectiveness revealing the superiority of the method (Castillo et al.,
268 2012). Also for a gully system, Stöcker et al. (2015) demonstrated the flexibility of camera
269 based surface reconstruction by combining independently captured terrestrial images with
270 surface models from UAV images to fill data gaps and achieve a comprehensive 3D model.
271 Large areal coverage and very high resolution allowed for a new quality in the assessment of
272 plot based soil erosion analysis (Eltner et al., 2015)

273 Another 6 studies tackle the 3D reconstruction of soil micro-topography by producing very
274 dense point clouds or DEMs. This data further serves to assess pros and cons of SfM
275 photogrammetry, e.g. to detect small-scale erosion features (Nouwakpo et al., 2014), with
276 regard to the doming effect (Eltner and Schneider, 2015) or as input parameter for erosion
277 modelling (Kaiser et al., 2015).

278

279 **3.2 Volcanology**

280 Volcanology is a pioneering area of SfM photogrammetry research in geosciences because 3
281 out of 6 studies in 2012 included volcanic research sites. James and Robson (2012) acquired
282 information on volcanic dome volume and structural variability prior to an explosion from
283 multi-temporal imagery taken from a light airplane. Another interesting work by Bretar et al.
284 (2013) successfully reveals roughness differences in volcanic surfaces from lapilli deposits to
285 slabby pahoehoe lava.

286

287 **3.3 Glaciology**

288 Glaciology and associated moraines are examined in 7 publications. In several UAV
289 campaigns Immerzeel et al. (2014) detected limited mass losses and low surface velocities but
290 high local variations of melt rates that are linked to supra-glacial ponds and ice cliffs. Rippin

291 et al. (2015) present another UAV-based work on supra-glacial runoff networks, comparing
292 the drainage system to surface roughness and surface reflectance measurements and detecting
293 linkages between all three. Furthermore, snow depth estimation and rock glacier monitoring
294 are increasingly performed with SfM photogrammetry (Nolan et al., 2015, Dall'Asta et al.,
295 2015).

296

297 **3.4 Mass movements**

298 Compared to the well-established use of LiDAR techniques on the investigation of landslides
299 (Jaboyedoff et al., 2012) the use of photogrammetric workflows for investigating hazardous
300 slopes is still scarce, which is probably due to the stringent accuracy and safety requirements.
301 For instance, the use of UAV systems for monitoring mass movements using both image
302 correlation algorithms and DEM subtraction techniques has been explored by Lucieer et al.,
303 (2013). More recently, SfM techniques were used by Stumpf et al. (2014) for monitoring
304 landslide displacements and erosion during several measuring campaigns, including the study
305 of seasonal dynamics on the landslide body, superficial deformation and rock fall occurrence.
306 In addition, these authors assessed the accuracy of two different 3D reconstruction tools
307 compared to LiDAR data.

308

309 **3.5 Fluvial morphology**

310 Channel networks in floodplains were surveyed by Prosdocimi et al. (2015) in order to
311 analyse eroded channel banks and to quantify the transported material. Besides classic DSLR
312 cameras, evaluation of an iPhone camera revealed sufficient accuracy, so that in near future
313 also non-scientist will be able to carry out post event documentation of damage. An
314 interesting large scale riverscape assessment is presented by Dietrich (2016), who carried out
315 a helicopter based data acquisition of a 32 km river segment. A small helicopter proves to
316 close the gap between unmanned platforms and commercial aerial photography from
317 airplanes.

318

319 **3.6 Coastal morphology**

320 In the article by Westoby et al. (2012) several morphological features of contrasting
321 landscapes were chosen to test the capabilities of SfM; one of them being a coastal cliff of
322 roughly 80 m height. Up to 90.000 points/m² enabled the identification of bedrock faulting.

323 Ružić et al. (2014) produced surface models of coastal cliffs to test the abilities of SfM
324 photogrammetry in undercuts and complex morphologies.

325

326 **3.7 Other fields of investigation in geosciences**

327 In addition to the prevalent fields of attention also more exotic research is carried out
328 unveiling unexpected possibilities for SfM photogrammetry. Besides the benefit for the
329 specific research itself, these branches are important as they either explore new frontiers in
330 geomorphometry or demonstrate the versatility of the method. Lucieer et al. (2014) analyse
331 arctic moss beds and their health conditions by using high-resolution surface topography
332 (2 cm DEM) to simulate water availability from snow melt. Leon et al. (2015) acquired
333 underwater imagery of a coral reef to produce a DEM with a resolution of 1 mm for
334 roughness estimation. Genchi et al. (2015) used UAV-image data of an urban cliff structure to
335 identify bio erosion features and found a pattern in preferential locations.

336 The re-consideration of historical aerial images is another interesting opportunity arising from
337 the new algorithmic image matching developments that allow for new DEM resolutions and
338 thus possible new insights into landscape evolution (Gomez et al., 2015).

339

340 **4 Error assessment of SfM photogrammetry in geo-scientific applications**

341 SfM photogrammetry has been tested under a large variety of environments due to the
342 commensurate novel establishment of the method in geosciences, revealing numerous
343 advantages but also disadvantages regarding to each application. It is important to have
344 method independent references to evaluate 3D reconstruction tools confidently. In total 39
345 studies are investigated (Table Appendix A), where a reference has been setup, either area
346 based (e.g. TLS) or point based (e.g. RTK GPS points). Because not all studies perform
347 accuracy assessment with independent references, the number of studies is in contrast to the
348 number of 65 studies that are reviewed in regard to applications. In the following, methods are
349 illustrated concerning integrated consideration of error performance of SfM photogrammetry
350 in geo-scientific studies.

351 A designation of error parameters is performed prior to comparing the studies to avoid using
352 ambiguous terms. There is a difference between local surface quality and more systematic
353 errors, i.e. due to referencing and project geometry (James and Robson, 2012). Specifically,
354 error can be assessed in regard to accuracy and precision.

355 Measurement accuracy, which defines the closeness of the measurement to a reference,
356 ideally displays the true surface and can be estimated by the mean error value. However,
357 positive and negative deviations can compensate for each other and thus can impede the
358 recognition of a systematic error (e.g. symmetric tilting) with the mean value. Therefore,
359 numerical and spatial error distribution should also be considered to investigate the quality of
360 the measurement (e.g. Smith et al., 2015). For the evaluation of two DEMs, the iterative
361 closest point (ICP) algorithm can improve the accuracy significantly if a systematic linear
362 error (e.g. shifts, tilts or scale variations) is given, as demonstrated by Micheletti et al. (2014);
363 Nevertheless, this procedure can also induce an error when the scene has changed
364 significantly between the two datasets.

365 Precision, which defines the repeatability of the measurement, e.g. it indicates how rough an
366 actual planar surface is represented, usually comprises random errors that can be measured
367 with the standard deviation or RMSE. However, precision is not independent from systematic
368 errors. In this study, the focus lies on RMSE or standard deviation calculated to a given
369 reference (e.g. to a LiDAR - light detection and ranging - point cloud) and thus the general
370 term “measured error” is used.

371 Furthermore, error ratios are calculated to compare SfM photogrammetry performance
372 between different studies under varying data acquisition and processing conditions. Thereby,
373 the relative error (e_r), the reference superiority (e_s) and the theoretical error ratio (e_t) are
374 considered. The first is defined as the ratio between measured error and surface to camera
375 distance (eq. 1).

$$376 \quad e_r = \frac{\sigma_m}{D} \quad (1)$$

377 Being:

e_r ...relative error

σ_m ...measured error

D ...mean distance camera – surface

378

379 The reference superiority displays the ratio between the measured error and the error of the
380 reference (eq. 2). It depicts the validity of the reference to be accountable as a reliable dataset
381 for comparison.

$$382 \quad e_s = \frac{\sigma_m}{\sigma_{ref}} \quad (2)$$

383 Being:

e_r ... *reference superiority*

σ_{ref} ... *reference error*

384

385 The theoretical error ratio includes the theoretical error, which is an estimate of the
386 theoretically best achievable photogrammetric performance under ideal conditions. It is
387 calculated separately for convergent and parallel-axes image acquisition schemes. The
388 estimate of the theoretical error of depth measurement for the parallel-axis case is displayed
389 by eq. 3 (more detail in Kraus, 2007). The error is determined for a stereo-image pair and thus
390 might overestimate the error for multi-view reconstruction. Basically, the error is influenced
391 by the focal length, the camera-to-surface distance and the distance between the images of the
392 stereo-pair (base).

$$393 \quad \sigma_p = \frac{D^2}{Bc} \sigma_i \quad (3)$$

394 Being:

σ_p ... *coordinate error for parallel – axes case*

c ... *focal length*

σ_i ... *error image measurement*

395 B ... *distance between images (base)*

396

397 For the convergent case the error also considers the camera-to-surface distance and the focal
398 length. However, instead of the base the strength of image configuration determined by the
399 angle between intersecting homologous rays is integrated and additionally the employed
400 number of images is accounted for (eq. 4; more detail in Luhmann et al., 2014).

$$401 \quad \sigma_c = \frac{qD}{\sqrt{kc}} \sigma_i \quad (4)$$

402 Being:

σ_c ... *coordinate error for convergent case*

q ... *strength of image configuration, i. e. convergence*

k ... *number of images*

403

404 Finally, the theoretical error ratio is calculated displaying the relation between the measured
405 error and the theoretical error (eq. 5). The value depicts the performance of SfM
406 photogrammetry in regard to the expected accuracy.

407
$$e_t = \frac{\sigma_m}{\sigma_{theo}} \tag{5}$$

408 Being:

409 e_t ... *theoretical error ratio*

σ_{theo} ... *theoretical error; either σ_p or σ_c*

410

411 The statistical analysis of the achieved precisions of the reviewed studies is performed with
412 the Python Data Analysis Library (pandas). If several errors are given in one study due to
413 testing of different survey or processing conditions, the error value representing the
414 enhancement of the SfM performance has been chosen, i.e. in the study of Javernick et al.
415 (2014) the DEM without an error dome, in the study of Rippin et al. (2015) the linear
416 corrected DEM, and in the study of Eltner & Schneider (2015) the DEMs calculated with
417 undistorted images. In addition, if several approaches are conducted to retrieve the deviations
418 value to the reference, the more reliable error measure is preferred (regards Stumpf et al.,
419 2014 and Gómez-Gutiérrez et al., 2014 and 2015). Apart from those considerations, measured
420 errors have been averaged if several values are reported in one study, i.e. concerning multi-
421 temporal assessments or consideration of multiple surfaces with similar characteristics, but
422 not for the case of different tested SfM tools. Regarding data visualisation, outliers that
423 complicated plot drawing, were neglected within the concerning graphics. This concerned the
424 study of Dietrich (2016) due to a very large scale of an investigated river reach (excluded
425 from Fig. 4a and Fig. 5a-b), the study of Snapir et al. (2014) due to a very high reference
426 accuracy of Lego bricks (excluded from Fig. 4c and Fig. 5b), and Frankl et al. (2015) due to a
427 high measured error as the study focus was rather on feasibility than accuracy (excluded from
428 Fig. 5c).

429 Besides exploiting a reference to estimate the performance of the 3D reconstruction,
430 registration residuals of GCPs resulting from BA can be taken into account for a first error
431 assessment. But this is not suitable as an exclusive error measure due to potential deviations
432 between the true surface and the calculated statistical and geometric model, which are not
433 detectable with the GCP error vectors alone because BA is optimised to minimise the error at
434 these positions. However, if BA has been performed two-staged (i.e. SfM and referencing
435 calculated separately), the residual vector provides reliable quality information because
436 registration points are not integrated into model estimation.

437 Error evaluation in this study is performed with reference measurements. Thereby, errors due
438 to the performance of the method itself and errors due to the method of quality assessment
439 have to be distinguished.

440

441 **4.1 Error sources of SfM photogrammetry**

442 The error of 3D reconstruction is influenced by many factors: scale/distance, camera
443 calibration, image network geometry, image matching performance, surface texture and
444 lighting conditions, and GCP characteristics, which are examined in detail in this section.

445

446 **4.1.1 Scale and sensor to surface distance**

447 SfM photogrammetry contains the advantage to be useable at almost any scale. Thus, in the
448 reviewed studies the method is applied at a large range of scales (Fig. 4a), reaching from
449 10 cm for volcanic bombs (Favalli et al., 2012, James and Robson, 2012) up to 10 km for a
450 river reach (Dietrich, 2016). Median scale amounts to about 100 m. SfM photogrammetry
451 reveals a scale dependent practicability (Smith and Vericat, 2015) if case study specific
452 tolerable errors are considered, e.g. for multi-temporal assessments. For instance, at plot and
453 hillslope scale 3D reconstruction is a very sufficient method for soil erosion studies, even
454 outperforming TLS (Nouwakpo et al., 2015, Eltner et al., 2015, Smith and Vericat, 2015). The
455 method should be most useful in small scale study reaches (Fonstad et al., 2013), whereas
456 error behaviour is not as advantageous for larger scales, i.e. catchments (Smith and Vericat,
457 2015).

458 Besides scale, the distance between sensor and surface is important for image-based
459 reconstructed DEM error, also because scale and distance interrelate. The comparison of the
460 reviewed studies indicates that with an increase of distance the measured error increases,
461 which is not unexpected (Fig. 5a, circles). However, there is no linear trend detectable.
462 Therefore, the relative error is not assignable. The relative error displays a large range from
463 15 to 4000 with a median of 400, thus revealing a rather low error potential (Fig. 5a,
464 triangles). Very high ratios are solely observable for very close-range applications and at large
465 distances. A general increase of the relative error with distance is observable (Fig. 5a,
466 triangles). The indication that cm-accurate measurements are realisable at distances below
467 200 m (Stumpf et al., 2014) can be confirmed by Fig. 5a because most deviations are below

468 10 cm up to that range. Overall, absolute error values are low at close ranges, whereas the
469 relative error is higher at larger distances.

470

471 **4.1.2 Camera calibration**

472 SfM photogrammetry allows for straight forward handling of camera options due to integrated
473 self-calibration, but knowledge about some basic parameters is necessary to avoid unwanted
474 error propagation into the final DEM from insufficiently estimated camera models. The
475 autofocus as well as automatic camera stabilisation options should be deactivated if a pre-
476 calibrated camera model is used or one camera model is estimated for the entire image block
477 because changes in the interior camera geometry due to camera movement cannot be captured
478 with these settings. The estimation of a single camera model for one image block is usually
479 preferable, if a single camera has been used, whose interior geometry is temporary stable, to
480 avoid over-parameterisation (Pierrot-Deseilligny and Clery, 2011). Thus, if zoom lenses are
481 moved a lot during data acquisition, they should be avoided due to their instable geometry
482 (Shortis et al., 2006, Sanz-Ablanedo et al., 2010) that impedes usage of pre-calibrated fixed or
483 single camera models. A good compromise between camera stability, sensor size and
484 equipment weight, which is more relevant for UAV applications, is achieved by compact
485 system cameras (Eltner and Schneider, 2015). However, solely three studies utilise compact
486 system cameras in the reviewed studies (Tonkin et al., 2014, Eltner and Schneider, 2015,
487 Eltner et al., 2015).

488 Along with camera settings, the complexity in regard to the considered parameters of the
489 defined camera model within the 3D reconstruction tool is relevant as well as the
490 implementation of GCPs to function as further observations in the BA, i.e. to avoid DEM
491 domes as a consequence of insufficient image distortion estimation (James and Robson, 2014,
492 Eltner and Schneider, 2015). Also, Stumpf et al. (2014) detect worse distortion correction
493 with a basic SfM tool, considering a simple camera model, compared to more complex
494 software, integrating a variety of camera models and GCP consideration. Camera calibration
495 is a key element for high DEM quality, which is extensively considered in photogrammetric
496 software, whereas simpler models that solely estimate principle distance and radial distortion
497 are usually implemented in the SfM tools originating from computer vision (Eltner and
498 Schneider, 2015, James and Robson, 2012, Pierrot-Deseilligny and Clery, 2011).

499

500 **4.1.3 Image resolution**

501 Image resolution is another factor influencing the final DEM quality. Especially, the absolute
502 pixel size needs to be accounted for due to its relevance for the signal-to-noise ratio (SNR)
503 because the larger the pixel the higher the amount of light that can be captured and hence a
504 more distinct signal is measured. Resolution alone by means of pixel number gives no
505 information about the actual metric sensor size. A large sensor with large pixels and a large
506 amount of pixels provides better image quality due to reduced image noise than a small sensor
507 with small pixels but the same amount of pixels. Thus, high image resolution defined by large
508 pixel numbers and pixel sizes resolves in sufficient quality of images and thus DEMs
509 (Micheletti et al., 2014, Eltner and Schneider, 2015).

510 However, the reviewed investigations indicate no obvious influence of the pixel size at the
511 DEM quality. Mostly, cameras with middle sized sensors and corresponding pixel sizes
512 around 5 μm are used and a large range of errors at different pixel sizes is given.

513 To speed up processing, down-sampling of images is often performed causing interpolation of
514 pixels and thus the reduction of image information, which can be the cause for
515 underestimation of high relief changes, e.g., observed by Smith and Vericat (2015) or
516 Nouwakpo et al. (2015). Interestingly, Prosdocimi et al. (2015) reveal that lower errors are
517 possible with decreasing resolution due to an increase of error smoothing. Nevertheless,
518 image data collection in the field should be done at highest realisable resolution and highest
519 SNR to fully keep control over subsequent data processing, i.e. data smoothing should be
520 performed under self-determined conditions at the desktop, which is especially important for
521 studies of rough surfaces to allow for probate error statistics (e.g. Brasington et al., 2012).

522

523 **4.1.4 Image network geometry**

524 In regard to the geometry of the image network several parameters are important: number of
525 images, image overlap, obliqueness and convergence.

526 At least three images need to capture the area of interest, but for redundancy and to decrease
527 DEM error higher numbers are preferred (James and Robson, 2012). For instance, Piermattei
528 et al. (2015) detect better qualities for a higher amount of images. However, the increase of
529 images does not linearly increase the accuracy (Micheletti et al., 2014), and may ultimately
530 lead to unnecessary increase in computation time. Generally, image number should be chosen
531 depending on the size and complexity of the study reach (James and Robson, 2012); as high
532 as possible but still keeping in mind acceptable processing time.

533 High image overlap is relevant to finding homologous points within many images that cover
534 the entire image space. Stumpf et al. (2014) show that higher overlap resolves in better
535 results. Wide angle lenses, whose radial distortion is within the limits, should be chosen for
536 data acquisition.

537 The reviewed studies reveal a large variety of applicable perspectives for DEM generation.
538 Most applications use images captured from the ground, which is the most flexible
539 implementation of the SfM photogrammetry method. In regard to terrestrial or aerial
540 perspective, Smith and Vericat (2015) state that aerial images should be preferred if plots
541 reach sizes larger than 100 m because at these distances obliqueness of images becomes too
542 adverse. Stumpf et al. (2014) even mention a distinct value of the incidence angle of 30° to
543 the captured surface above which data quality decreases significantly.

544 Furthermore, image network geometry has to be considered separately for convergent
545 acquisitions schemes, common for terrestrial data collection, and for parallel-axes acquisition
546 schemes, common for aerial data collection. The parallel-axes image configuration results in
547 unfavourable error propagation due to unfavourable parameter correlation, which inherits the
548 separation between DEM shape and radial distortion (James and Robson, 2014, Wu, 2014)
549 resulting in a dome error that needs either GCP implementation or a well estimated camera
550 model for error mitigation (James and Robson, 2014, Eltner and Schneider, 2015). However,
551 GCP accuracy has to be sufficient or else the weight of GCP information during BA is too
552 low to avoid unfavourable correlations, as shown by Dietrich (2016), where DEM dome error
553 within a river reach could not be diminished even though GCPs were implemented into 3D
554 reconstruction. If convergent images are utilised, the angle of convergence is important
555 because the higher the angle the better the image network geometry. Thereby, accuracy
556 increases because sufficient image overlap is possible with larger bases between images.
557 Therefore, glancing ray intersections, which impede distinct depth assignment, are avoided.
558 But simultaneously, convergence should not be so high that the imaged scene becomes too
559 contradictory for successful image matching (Pierrot-Deseilligny and Clery, 2012, Stöcker et
560 al, 2015).

561

562 **4.1.5 Accuracy and distribution of homologues image points**

563 The quality of DEMs reconstructed from overlapping images depends significantly on the
564 image-matching performance (Grün, 2012). Image content and type, which cannot be
565 enhanced substantially, are the primary factors controlling the success of image-matching

566 (Grün, 2012). Image-matching is important for reconstruction of the image network geometry
567 as well as the subsequent dense-matching.

568 On the one hand, it is relevant to find good initial matches (e.g. SIFT features are not as
569 precise as least square matches with $\frac{1}{10}$ pixel size accuracies; Grün, 2012) to perform reliable
570 3D reconstruction and thus retrieve an accurate sparse point cloud because optimization
571 procedures for model refinement rely on this first point cloud. Thus, immanent errors will
572 propagate along the different stages of SfM photogrammetry.

573 On the other hand, more obviously image-matching performance is important for dense
574 reconstruction, when 3D information is calculated for almost every pixel. The accuracy of
575 intersection during dense matching depends on the accuracy of the estimated camera
576 orientations (Remondino et al., 2014). If the quality of the DEM is the primary focus, which is
577 usually not the case for SfM algorithms originating from computer vision, the task of image-
578 matching is still difficult (Grün, 2012). Nevertheless, newer approaches are emerging, though,
579 which still need evaluation in respect of accuracy and reliability (Remondino et al., 2014). An
580 internal quality control for image-matching is important for DEM assessment (Grün, 2012),
581 but is mostly absent in tools for SfM photogrammetry.

582 So far, many studies exist, which evaluate the quality of 3D reconstruction in geo-scientific
583 applications. Nevertheless, considerations of dense-matching performance are still missing,
584 especially in regard of rough topographies (Eltner and Schneider, 2015).

585

586 **4.1.6 Surface texture**

587 Texture and contrast of the area of interest are significant to identify suitable homologous
588 image points. Low textured and contrasted surfaces result in a distinct decrease of image
589 features, i.e. snow covered glaciers (Gómez-Gutiérrez et al., 2014) or sandy beaches (Mancini
590 et al., 2013). Furthermore, vegetation cover complicates image matching performance due to
591 its highly variable appearance from differing viewing angles (e.g. Castillo et al., 2012, Eltner
592 et al., 2015) and possible movements during wind. Thus, in this study, where present, only
593 studies of bare surfaces are reviewed for error assessment.

594

595 **4.1.7 Illumination condition**

596 Over- and under-exposure of images is another cause of error in the reconstructed point cloud,
597 which cannot be significantly improved by utilising HDR images (Gómez-Gutiérrez et al.,
598 2015). Well illuminated surfaces result in a high number of detected image features, which is
599 demonstrated for coastal boulders under varying light conditions by Gienko and Terry (2014).
600 Furthermore, Gómez-Gutiérrez et al. (2014) highlight the unfavourable influence of shadows
601 because highest errors are measured in these regions; interestingly, these authors calculate the
602 optimal time for image acquisition from the first DEM for multi-temporal data acquisition.
603 Furthermore, the temporal length of image acquisition needs to be considered during sunny
604 conditions because with increasing duration shadow changes can decrease matching
605 performance, i.e. with regard to the intended quality surveys lasting more than 30 minutes
606 should be avoided (Bemis et al., 2014). Generally, overcast but bright days are most suitable
607 for image capture to avoid strong shadows or glared surfaces (James and Robson, 2012).

608

609 **4.1.8 GCP accuracy and distribution**

610 GCPs are important inputs for data referencing and scaling. Photogrammetry always stresses
611 the weight of good ground control for accurate DEM calculation, especially if one-staged BA
612 is performed. In the common SfM workflow integration of GCPs is less demanding because
613 they are only needed to transform the 3D-model from the arbitrary coordinate system, which
614 is comparable to the photogrammetric two-staged BA processing. A minimum of three GCPs
615 are necessary to account for model rotation, translation and scale. However, GCP redundancy,
616 i.e. more points, has been shown to be preferable to increase accuracy (James and Robson,
617 2012). A high number of GCPs further ensures the consideration of checkpoints not included
618 for the referencing, which are used as independent quality measure of the final DEM. More
619 complex 3D reconstruction tools either expand the original 3D-Helmert-transformation by
620 secondary refinement of the estimated interior and exterior camera geometry to account for
621 non-linear errors (e.g. Agisoft PhotoScan) or integrate the ground control into the BA (e.g.
622 APERO). For instance, Javernick et al. (2014) could reduce the height error to decimetre level
623 by including GCPs in the model refinement.

624 Natural features over stable areas, which are explicitly identifiable, are an alternative for GCP
625 distributions, although they usually lack strong contrast (as opposed to artificial GCPs) that
626 would allow for automatic identification and sub-pixel accurate measurement (e.g. Eltner et
627 al., 2013). Nevertheless, they can be suitable for multi-temporal change detection
628 applications, where installation of artificial GCPs might not be possible (e.g. glacier surface

629 reconstruction; Piermattei et al., 2015) or necessary as in some cases relative accuracy is
630 preferred over absolute performance (e.g. observation of landslide movements, Turner et al.,
631 2015).

632 GCP distribution needs to be even and adapted to the terrain resulting in more GCPs in areas
633 with large changes in relief (Harwin and Lucieer, 2012) to cover different terrain types.
634 Harwin and Lucieer (2012) state an optimal GCP distance between $\frac{1}{5}$ and $\frac{1}{10}$ of object distance
635 for UAV applications. Furthermore, the GCPs should be distributed widely across the target
636 area (Smith et al., 2015) and at the edge or outside the study reach (James and Robson, 2012)
637 to enclose the area of interest, because if the study area is extended outside the GCP area, a
638 significant increase of error is observable in that region (Smith et al., 2014, Javernick et al.,
639 2014, Rippin et al., 2015). If data acquisition is performed with parallel-axis UAV images and
640 GCPs are implemented for model refinement, rules for GCP setup according to classical
641 photogrammetry apply, i.e. dense GCP installation around the area of interest and height
642 control points in specific distances as function of image number (more detail in e.g. Kraus,
643 2007).

644 The measurement of GCPs can be performed either within the point cloud or the images,
645 preferring the latter because identification of distinct points in 3D point clouds of varying
646 density can be less reliable (James and Robson, 2012, Harwin and Lucieer, 2012) compared to
647 sub-pixel measurement in 2D images, where accuracy of GCP identification basically
648 depends on image quality. Fig. 5 illustrates that only few studies measured GCPs in point
649 clouds producing higher errors compared to other applications at the same distance.

650

651 **4.2 Errors due to accuracy/precision assessment technique**

652 **4.2.1 Reference of superior accuracy**

653 It is difficult to find a suitable reference for error assessment of SfM photogrammetry in geo-
654 scientific or geomorphologic applications due to the usually complex and rough nature of the
655 studied surfaces. So far, either point based or area based measurements are carried out. On the
656 one hand, point based methods (e.g. RTK GPS or total station) ensure superior accuracy but
657 lack sufficient area coverage for precision statements of local deviations; on the other hand,
658 area based (e.g. TLS) estimations are used, which provide enough data density but can lack of
659 sufficient accuracy (Eltner and Schneider, 2015). Roughness is the least constrained error
660 within point clouds (Lague et al., 2013) independent from the observation method. Thus, it is

661 difficult to distinguish between method noises and actual signal of method differences,
662 especially at scales where the reference method reaches its performance limit. For instance,
663 Tonkin et al. (2014) indicate that the quality of total station points is not necessarily superior
664 on steep terrain.

665 Generally, 75 % of the investigations reveal a measured error that is 20 times higher than the
666 error of the reference. But the median shows that the superiority of the reference accuracy is
667 actually significantly poorer; the measured error is merely twice the reference error (Fig. 4 c).
668 The reviewed studies further indicate that the superior accuracy of the reference seems to
669 depend on the camera-to-object distance (Fig. 5 b). At shorter distances (below 50 m) most
670 references reveal accuracies that are lower than one magnitude superiority to the measured
671 error. However, alternative reference methods are yet absent. Solely, for applications in
672 further distances the references are sufficient. These findings are relevant for the
673 interpretation of the relative error because low ratios at small scale reaches might be due to
674 the low performance of the reference rather than the actual 3D reconstruction quality but due
675 to the reference noise lower errors are not detectable. Low relative errors are measured where
676 the superior accuracy is also low (distance 5-50 m) and large ratios are given at distance
677 where superior accuracy increases as well.

678

679 **4.2.2 Type of deviation measurement**

680 The reviewed studies use different approaches to measure the distance between the reference
681 and the 3D reconstructed surface. Comparisons are either performed in 2.5D (raster) or real
682 3D (point cloud). Lague et al. (2013) highlight that the application of raster inherits the
683 disadvantage of data interpolation, especially relevant for rough surfaces or complex areas
684 (e.g. undercuts as demonstrated for gullies by Frankl et al., 2015). In this context it is
685 important to note that lower errors are measured for point-to-point distances rather than raster
686 differencing (Smith and Vericat, 2015, Gómez-Guérrez et al., 2014b).

687 Furthermore, within 3D evaluation different methods for deviation measurement exist. The
688 point-to-point comparison is solely suitable for a preliminary error assessment because this
689 method is prone to outliers and differing point densities. By point cloud interpolation alone
690 (point-to-mesh), this issue is not solvable because there are still problems at very rough
691 surfaces (Lague et al., 2013). Different solutions have been proposed: On the one hand,
692 Abellan et al. (2009) proposed averaging the point cloud difference along the spatial
693 dimension, which can also be extended to 4D (x, y, z, time; Kromer et al., 2015). On the other

694 hand, Lague et al. (2013) proposed the M3C2 algorithm for point cloud comparison that
695 considers the local roughness and further computes the statistical significance of detected
696 changes. Stumpf et al. (2014) and Gómez-Gutiérrez et al. (2015) illustrated lower error
697 measurements with M3C2 compared to point-to-point or point-to-mesh. Furthermore, Kromer
698 et al. (2015) showed how the 4D filtering, when its implementation is feasible, allows to
699 considerably increase the level of detection compared to other well-established techniques of
700 comparison.

701

702 **4.3 Standardised error assessment**

703 To compare the achieved accuracies and precisions of different studies a standardised error
704 assessment is necessary, e.g. considering the theoretical error ratio. The calculation of the
705 theoretical error for the convergent image acquisition schemes is possible, making some basic
706 assumptions about the network geometry, i.e. the strength of image configuration equals 1 (as
707 in James & Robson, 2012), the number of images equals 3 (as in James & Robson, 2012) and
708 an image measurement error of 0.29 due to quantisation noise (as a result of continuous signal
709 conversion to discrete pixel value). However, it is not possible to evaluate the theoretical error
710 for parallel-axes case studies because information about the distance between subsequent
711 images (base) is mostly missing, but essential to solve the equation and should not be
712 assumed. Eltner and Schneider (2015) and Eltner et al. (2015) compare their results to
713 parallel-axes theoretical error and demonstrate that for soil surface measurement from low
714 flying heights at least photogrammetric accuracy is possible (e.g. sub-cm error for altitudes
715 around 10 m).

716 The results from James and Robson (2012), which show a less reliable performance of SfM
717 than expected from photogrammetric estimation, can be confirmed by the reviewed studies.
718 Image-based 3D reconstruction, considering SfM workflows, performs poorer than the
719 theoretical error (Fig. 5c). The measured error is always higher and on average 90 times worse
720 than the theoretical error. Even for the smallest theoretical error ratio the actual error is 6
721 times higher. Furthermore, it seems that with increasing distance theoretical and measured
722 errors converge slightly.

723 As demonstrated, diverse factors influence SfM photogrammetry performance and subsequent
724 DEM error with different sensitivity. Generally, accurate and extensive data acquisition is
725 necessary to minimise error significantly (Javernick et al., 2014). Independent reference
726 sources, such as TLS, are not replaceable (James and Robson, 2012) due to their differing

727 error properties (i.e. error reliability) compared to image-matching (Grün, 2012). Synergetic
728 effects of SfM and classical photogrammetry should be used, i.e. benefiting from the high
729 automation of SfM to retrieve initial estimates without any prior knowledge about the image
730 scene and acquisition configuration and adjacent reducing error by approved photogrammetric
731 approaches, which are optimised for high accuracies.

732 The reviewed studies indicate the necessity of a standardised protocol for error assessment
733 because the variety of studies inherit a variety of scales worked at, software used, GCP types
734 measured, deviation measures applied, image network configurations implemented, cameras
735 and platforms operated and reference utilised, making it very difficult to compare results with
736 consistency. Relevant parameters for a standard protocol are suggested in Table 5.

737

738 **5 Perspectives and limitations**

739 SfM photogrammetry has allowed capturing massive three-dimensional datasets by non-
740 specialists during the last five years, and it is highly expected that this technique will evolve
741 during the forthcoming decade. Current studies are focusing on capturing the terrain's
742 geometry with high precision, but several opportunities to improve our understanding,
743 modelling and prediction of different earth surface processes still remain unexplored. For
744 instance, the use of super-macro imagery in conventional SfM workflows is expected to be
745 explored soon for investigating natural phenomena in a much higher level of detail.
746 Nevertheless, some technological issues that need to be addressed include the progressive
747 degradation of the data quality at very short distances due to the effect of a limited depth of
748 field; Up to our knowledge, the use of focus stacking for extending shallow depth of field of
749 single images has not been explored yet. Some other technical and operational aspects are still
750 limiting our ability to derive 3D point clouds from digital imagery over naturally complex
751 outcrops. Examples include the occurrence of biases and occlusions that can strongly
752 influence the quality of the acquired datasets and the progressive reduction of the ground
753 resolution (meter/pixel) at longer distances, which can be addressed using mobile platforms
754 such as UAV systems. Eventually, SfM photogrammetry technique may become a
755 mainstream procedure in geomorphological studies during the next decade, perspectives
756 include efforts in cross-disciplinarity, process automation, data and code sharing, real time
757 data acquisition and processing, unlocking the archives, etc., as follows:

758

759 **5.1 Cross-disciplinarity**

760 A great potential relies on adapting three dimensional methods originally developed for the
761 treatment of 3D LiDAR data to investigate natural phenomena through SfM photogrammetry
762 techniques. Applications on 3D point cloud treatment dating back to the last decade will soon
763 be integrated into SfM photogrammetry post-processing; Examples include:
764 geomorphological investigations in high mountain areas (Milan et al., 2007), geological
765 mapping (Buckley et al., 2008; Franceschi et al. 2009), soil erosion studies (Eltner and
766 Baumgart, 2015), investigation of fluvial systems (Heritage and Hetherington, 2007, Cavalli
767 et al., 2008; Brasington et al., 2012), and mass wasting phenomena (Lim et al., 2005,
768 Oppikofer et al. 2009, Abellan et al., 2010).

769 Some other data treatment techniques that have been developed during the last decade and
770 that will be adapted and enriched by the growing SfM photogrammetry community include:
771 automatic lithological segmentation according to the intensity signature (Humair et al., 2015),
772 integration of ground based LiDAR with thermal/hyperspectral imaging for lithological
773 discrimination (Kääb, 2008, Hartzell et al., 2014), extraction of the structural settings on a
774 given outcrop (Jaboyedoff et al., 2007, Sturzenegger and Stead, 2009, Gigli and Casagli,
775 2011, Riquelme et al., 2014) and the automatic extraction of geological patterns such as
776 surface roughness (Poropat, 2009), discontinuity spacing/persistence/waviness (Fekete et al.
777 2010, Khoshelham et al., 2011, Pollyea and Fairley, 2011). Concerning 4D data treatment for
778 investigating changes on natural slope, some lessons learned may be adapted from the bi- and
779 three-dimensional tracking of mass movements (Teza et al., 2007, Monserrat and Crosetto
780 2008), investigation of progressive failures (Royan et al., 2015, Kromer et al., 2015), and
781 from the usage of mobile systems (Lato et al., 2009, Michoud et al., 2015).

782

783 **5.2 Data and code sharing**

784 Open data in geomorphometric studies using point clouds is also needed. The development of
785 open-source software for handling huge 3D datasets such as CloudCompare (Girardeau-
786 Montaut, 2015) has considerably boosted geomorphometric studies using 3D point clouds due
787 to providing facile processing of such memory intense data. Nevertheless, appart from the
788 above mentioned case, sharing the source code or the RAW data of specific applications for
789 investigating earth surface processes is still not well-established in our discipline. A series of
790 freely available databases exist for LiDAR datasets (openTopography.org, rockbench.com,
791 3D-landslide.com). But to the knowledge of the authors, there is no specific Git-Hub cluster

792 or website dedicated to the maintaining and development of open-access software in
793 geosciences.

794

795 **5.3 Unlocking the archive**

796 The appraisal of digital photography and the exponential increase of data storage capabilities
797 have enabled the massive archive of optical images around the world. Accessing such
798 quantity of information could provide unexpected opportunities for the four dimensional
799 research of geomorphological processes using SfM photogrammetry workflows. Except for
800 some open repositories (e.g. Flickr, Google Street View) the possibility to access the massive
801 optical data is still scarce. In addition, accessing to such databases may become a challenging
802 task due to data interchangeability issues. A considerable effort may be necessary for creating
803 such a database with homogeneous data formats and descriptors (type of phenomenon,
804 temporal resolution, pixel size, accuracy, distance to object, existence of GCPs, etc.) during
805 the forthcoming years.

806 A first valuable approach to use data from online imagery was presented by Martin-Brualla et
807 al. (2015), who pave the way for further research in a new field of 3D surface analysis (i.e.
808 time-lapse). Other possible applications might unlock the archive of ancient airborne,
809 helicopter-based or terrestrial imagery, ranging from the estimation of coastal retreat rates,
810 the observation of the evolution of natural hazards to the monitoring of glacier fronts, and
811 further.

812

813 **5.4 Real time data acquisition**

814 Rapid developments in automation (soft- and hardware wise) allow for in situ data acquisition
815 and its immediate transfer to processing and analysing institutions. Thus, extreme events are
816 recognisable during their occurrence and authorities or rescue teams can be informed in real-
817 time. In this context SfM photogrammetry could help to detect and quantify rapid volume
818 changes of e.g. glacier fronts, pro-glacial lakes, rock failures and ephemeral rivers.

819 Furthermore, real-time crowd sourcing offers an entirely new dimension of data acquisition.
820 Due to the high connectivity of the public through smartphones, various possibilities arise to
821 share data (Johnson-Roberson et al., 2015). An already implemented example is real-time
822 traffic information. Jackson and Magro (2015) name further options. Crowd sourced imagery
823 can largely expand possibilities to 3D information.

824

825 **5.5 Time-lapse photography**

826 A limited frequency of data acquisition increases the likelihood of superimposition and
827 coalescence of geomorphological processes (Abellan et al., 2014). Since time-lapse SfM
828 photogrammetry data acquisition has remained so far unexplored, a great prospect is expected
829 on this topic during the coming years. To date solely James and Robson (2014b) demonstrated
830 its potential by monitoring a lava flow at minute intervals for 37 minutes. One reason why
831 time-lapse SfM photogrammetry remains rather untouched in geosciences lies in the complex
832 nature of producing continuous data sets.

833 Besides the need for an adequate research site (frequent morphodynamic activity), other
834 aspects have to be taken into account: an automatic camera setup is required with self-
835 contained energy supply (either via insolation or wind), adequate storage and appropriate
836 choice of viewing angles onto the area of interest. Furthermore, cameras need to comprise
837 sufficient image overlap and have to be synchronised. Ground control is required and an
838 automatic pipeline for large data treatment should be developed.

839 New algorithms are necessary to deal with massive point cloud databases. Thus, innovative
840 four dimensional approaches have to be developed to take advantage of the information
841 contained in real-time and/or time-lapse monitoring. Furthermore, handling huge databases is
842 an important issue and although fully automatic techniques may not be necessary in some
843 applications, a series of tedious and manual processes are still required for data treatment.
844 Combining real-time and/or time-lapse datasets with climatic information can improve the
845 modelling of geomorphological processes.

846

847 **5.6 Automatic UAV surveying**

848 Unmanned airborne vehicles already show a large degree of automation as they follow flight
849 paths and acquire data autonomously. Human control is not required except for launching of
850 the multi-copter or fixed wing system. Automatic landing is already provided by several
851 systems. In near future a fully automatic UAV installation could comprise the following:
852 repeated survey of an area of interest, landing and charging at a base station, data link for
853 local storage or satellite based data transfer, and safety mechanism for preventing lift-off
854 during inappropriate weather conditions. However, a large limitation for such a realisation lies
855 in legal restrictions because national authorities commonly request for visual contact to the

856 UAV in case of failure. But in remote areas installation of an automatic system could already
857 be allowed by regulation authorities.

858

859 **5.7 Direct geo-referencing**

860 The use of GCPs is very time-consuming in the current SfM workflow. At first, field efforts
861 are high to install and measure the GCPs during data acquisition. Afterwards, more time and
862 labour is required during post-processing in order to identify the GCPs in the images,
863 although some progress is made regarding to automatic GCP identification, e.g. by the
864 exploitation of templates (Chen et al., 2000). The efficiency of geo-referencing can be
865 increased significantly applying direct geo-referencing. Thus, the location and position of the
866 camera is measured in real time and synchronised to the image capture by an on-board GPS
867 receiver and an IMU (inertial measurement unit) recording camera tilts. This applies to UAV
868 systems as well as terrestrial data acquisition, e.g. by smartphones (Masiero et al., 2014).
869 Exploiting direct geo-referencing can reduce usage of GCPs to a minimum or even replace it,
870 which is already demonstrated by Nolan et al. (2015), who generated DEMs with spatial
871 extents of up to 40 km² and a geo-location accuracy of ± 30 cm.

872 The technique can be very advantageous when it comes to monitoring areas with great spatial
873 extents or inaccessible research sites. However, further development is necessary, thereby
874 focusing on light-weighted but precise GPS receivers and IMU systems; on UAVs due to their
875 limited payload and on hand-held devices due to their feasibility (e.g. Eling et al., 2015).

876

877

878 **6 Conclusions**

879 This review has shown the versatility and flexibility of the recently established method SfM
880 photogrammetry. Due to its beneficial qualities, a wide community of geoscientists starts to
881 implement 3D reconstruction based on images within a variety of studies. Summing up the
882 publications, there are no considerable disadvantages mentioned (e.g. accuracy wise)
883 compared to other methods that cannot be counteracted by placement of GCPs, camera
884 calibration or a high image number. Frontiers in geomorphometry have been expanded once
885 more, as limits of other surveying techniques such as restricted mobility, isolated area of
886 application and high costs are overcome by the SfM photogrammetry. Its major advantages lie

887 in easy-to-handle and cost-efficient digital cameras as well as non-commercial software
888 solutions.

889 SfM photogrammetry is already becoming an essential tool for digital surface mapping. It is
890 employable in a fully automatic manner but individual adjustments can be conducted to
891 account for each specific case study constrain and accuracy requirement in regard to the
892 intended application. Due to the possibility of different degrees of process interaction, non-
893 experts can utilise the method depending on their discretion.

894 While research of the last years mainly focussed on testing the applicability of SfM
895 photogrammetry in various geo-scientific applications, recent studies try to pave the way for
896 future usages and develop new tools, setups or algorithms. Performance analysis revealed the
897 suitability of SfM photogrammetry at a large range of scales in regard to case study specific
898 accuracy necessities. However, different factors influencing final DEM quality still need to be
899 addressed. This should be performed under strict experimental (laboratory) designs because
900 complex morphologies, typical in earth surface observations, impede accuracy assessment due
901 to missing superior reference. Thus, independent references and GCPs are still needed in SfM
902 photogrammetry for reliable estimation of the quality of each 3D reconstructed surface.

903

904 Fast and straightforward generation of DEMs using freely available tools produces new
905 challenges. The exploitation of the entire information of the SfM photogrammetry output (3D
906 point cloud or mesh instead of 2.5D raster) will become a significant challenge in future
907 studies of high resolution topography (Passalacqua et al., 2015), which has to be even
908 extended to 4D when investigating the evolution along time. Thus, especially comprehensive
909 end user software needs further progress in these aspects.

910

911 **Appendix A:**

912 Summary of information about reviewed studies used for application evaluation and performance assessment of SfM photogrammetry. Variables are
 913 explained in chapter 5.

ID	Author	Year	Application	Software	Perspective	Distance [m]	Scale* [m]	Pixel size [μm]	Image number	Complexity of SfM tool	Measurement error [mm]	Relative error	reference superiority	Theoretical error ratio
1	Castillo et al.	2012	gully erosion	Bundler + PMVS2	terrestrial	7	7	5.2	191	basic	20	350	-	79
2	Castillo et al.	2014	ephemeral gully erosion	Bundler + PMVS2	terrestrial	6	25	5.2	515	basic	22	273	11	101
3	Castillo et al.	2015	gully erosion	SF3M	terrestrial	10	350	1.5	3095	basic	69	145	3.45	455
4	Dietrich	2016	riverscape mapping	PhotoScan	helicopter	200	10000	4.3	1483	complex	730	274	-	-
5	Eltner et al.	2015	soil erosion	Pix4D	UAV	10	30	2.0, 5.0	100	complex	5, 6	2000, 1667	-	-
6	Eltner and Schneider	2015	soil roughness	VisualSfM + PMVS2, PhotoScan, Pix4D, APERO + MicMac, Bundler + PMVS2	UAV	12	15	5.0	13	basic, complex	8.1 - 9.8	1224 - 1481	-	-
7	Favalli et al.	2012	geological outcrops, volcanic bomb, stalagmite	Bundler + PMVS2	terrestrial	1	0.1 - 0.3	5.2	30 - 67	basic	0.3 - 3.8	367 - 3333	-	-
8	Fonstad et al.	2013	bedrock channel and floodplain	Photosynth (Bundler implementation)	terrestrial	40	200	1.7	304	basic	250	160	2	139
9	Frankl et al.	2015	gully	PhotoScan	terrestrial	2	10	5.2	180 -	complex	17 - 190	11 - 147	0 - 4	156 - 2184

			measurement					235						
10	Genchi et al.	2015	bioerosion pattern	VisualSfM + PMVS2	UAV	20	100	1.5	400	basic	35	571	-	29
11	Gómez-Gutiérrez et al.	2014	gully headcut	123D Catch	terrestrial	9.3 - 10.5	10	4.3	41 - 93	basic	12 - 32	291 - 792	-	31 - 85
12	Gómez-Gutiérrez et al.	2014	rock glacier	123D Catch	terrestrial	300	130	8.2	6	basic	430	698	72	103
13	Gómez-Gutiérrez et al.	2015	rock glacier	123D catch, PhotoScan	terrestrial	300	130	8.2	9	basic, complex	84 - 1029	-	-	-
14	Immerzeel et al.	2014	dynamic of debris covered glacial tongue	PhotoScan	UAV	300	3500	1.3	284, 307	complex	330	909	-	-
15	James and Robson	2012	volcanic bomb, summit crater, coastal cliff	Bundler + PMVS2	terrestrial, UAV	0.7 - 1000	0.1 - 1600	5.2, 7.4	133 - 210	basic	1000 - 2333	0 - 62	1 - 12	16 - 25
16	Javernick et al.	2014	braided river	PhotoScan	helicopter	700	1500	-	147	complex	170	4118	3	-
17	Johnson et al.	2014	alluvial fan, earthquake scarp	PhotoScan	UAV	50, 60	300, 1000	4.8	233, 450	complex	130 - 410	122 - 385	-	-
18	Kaiser et al.	2014	gully and rill erosion	PhotoScan	terrestrial	5	10	6.4	-	complex	73 - 141	35 - 68	-	232 - 447
19	Leon et al.	2015	coral reef roughness	PhotoScan	terrestrial (marine)	1.5	250	1.5	1370	complex	0.6	2500	-	-
20	Mancini et al.	2013	fore dune	PhotoScan	UAV	40	200	4.3	550	complex	110 - 190	211 - 364	4	-
21	Micheletti et al.	2014	river bank, alluvial fan	123D Catch	terrestrial	10, 345	10, 300	4.8, 1.8	13	complex	16.8 - 526.3	327 - 595	-	40 - 73
22	Nadal-Romero et al.	2015	badland erosion	PhotoScan	terrestrial	50, 125	50, 100	5.5	15, 17	complex	14 - 33	2500 - 4032	1 - 2	6 - 10

23	Nouwakpo et al.	2015	microtopography erosion plots	PhotoScan	terrestrial	2	6	6.4	25	complex	5	400	-	-
24	Ouédraogo et al.	2014	agricultural watershed	Apero + MicMac, PhotoScan	UAV	100	200	2.0	760	complex	90, 139	1111, 719	-	6, 9
25	Piermattei et al.	2015	debris covered glacier monitoring	PhotoScan	terrestrial	100	350	4.8, 6.3	35, 47	complex	300, 130	333, 769	2, 1	56, 35
26	Prosdocimi et al.	2015	channel bank erosion	PhotoScan	terrestrial	7	30	1.4 - 6.3	60	complex	57 - 78	90 - 123	1	143 - 373
27	Rippin et al.	2015	supra-glacial hydrology	PhotoScan	UAV	121	2000	2.2	423	complex	400	303	-	-
28	Ruzic et al.	2014	coastal cliff	Autodesk ReCap	terrestrial	15	50	2.0	250	basic	70	214	1	82
29	Smith et al.	2014	post-flash flood evaluation	PhotoScan	terrestrial	50	150	1.7	-	complex	135	370	14	39
30	Smith and Vericat	2015	badland changes at different scales	PhotoScan	terrestrial, UAV,	5 - 250	20 - 1000	1.7, 5.5	30 - 527	complex	12.8 - 445	132 - 974	2 - 89	36 - 107
31	Snapir et al.	2014	roughness of soil surface	SfMToolkit	terrestrial	0.6	3	4.3	700	basic	2.7	222	270	-
32	Stumpf et al.	2014	landslide scarp	VisualSfM + CMVS, APERO + MicMac	terrestrial	50	750	8.5	88 - 401	basic, complex	27 - 232	667 - 1852	1 - 3	13 - 64
33	Tamminga et al.	2015	change detection after extreme flood event	EnsoMOSAIC UAV	UAV	100	200	1.3	310	complex	47	2128	2	-
34	Tonkin et al.	2014	moraine-mound topography	PhotoScan	UAV	100	500	4.3	543	complex	517	193	-	-
35	Turner et al.	2015	landslide change detection	PhotoScan	UAV	40	125	4.3	62 - 415	complex	31 - 90	444 - 1290	1 - 3	-
36	Westoby et al.	2012	coastal cliff	SfMToolkit	terrestrial	15	300	4.3	889	basic	500	100	-	-
37	Westoby et al.	2014	moraine dam,	SfMToolkit3	terrestrial	500	500	4.3	1002,	basic	814, 85	614,	2, 43	-

	al.		alluvial debris fan					1054			1176			
38	Woodget et al.	2015	fluvial topography	PhotoScan	UAV	26 - 28	50, 100	2.0	32 - 64	complex	19 - 203	138 - 1421	-	-
39	Zarco-Tejada et al.	2014	tree height estimation	Pix4D	UAV	200	1000	4.3	1409	complex	350	571	23	-
40	Bemis et al.	2014	structural geology	PhotoScan	UAV, terrestrial	-	-	-	-	-	-	-	-	-
41	Bendig et al.	2013	crop growth	PhotoScan	UAV	30	7	-	-	-	-	-	-	-
42	Bini et al.	2014	coast erosion/abrasion	Bundler	terrestrial	-	-	-	-	-	-	-	-	-
43	Bretar et al.	2013	(volcanic) surface roughness	APER0 + MicMac	terrestrial	1.5	5.9 - 24.6	-	-	-	-	-	-	-
44	Brothelande et al.	2015	post-caldera resurgence	PhotoScan	aircraft	150	6000	8.2	7000	-	3100	48	62	-
45	Burns et al.	2015	coral reef	Photoscan	terrestrial (marine)	2	28	-	-	-	-	-	-	-
46	Clapuyt et al.	2015	slope morphology	VisualSFM	UAV	50	100	-	-	-	-	-	-	-
47	Dall'Asta et al.	2015	rock glacier monitoring	APER0 + MicMac, Photoscan	UAV	150		-	-	-	-	-	-	-
48	Dandois and Ellis	2013	vegetation mapping	Photoscan	UAV	130	250	-	-	-	-	-	-	-
49	Fernández et al.	2015	landslide	Photoscan	UAV	90	250	-	-	-	-	-	-	-
50	Gienko and Terry	2014	coastal boulders	Photoscan	terrestrial	3	2.5	-	-	-	-	-	-	-
51	Fugazza et al.	2015	glacier mapping	Menci APS	UAV	250	500	-	-	-	-	-	-	-
52	Gomez	2014	volcano morphology	Photoscan	aircraft	-	10000	-	-	-	-	-	-	-
53	Harwin and Lucieer	2012	coastal erosion	Bundler + PMVS2	UAV	120	100	-	1	-	-	-	-	-

54	James and Varley	2012	volcanic dome control	Bundler Photogrammetry package	aircraft	505 – 2420	250	-	-	-	-	-	-	-
55	Kaiser et al.	2015	soil hydraulic roughness	PhotoScan	terrestrial	0.5	1	-	-	-	-	-	-	-
56	Lucieer et al.	2013	landslide	PhotoScan	UAV	40	125	-	-	-	-	-	-	-
57	Lucieer et al.	2014	antartic moss beds	PhotoScan	UAV	50	64	-	-	-	-	-	-	-
58	Meesuk et al.	2014	Urban flooding	VisualSfM	terrestrial	-	-	-	-	-	-	-	-	-
59	Morgenroth and Gomez	2014	tree structure	Photoscan	terrestrial	5	5	-	-	-	-	-	-	-
60	Nouwakpo et al.	2014	soil microtopography	Photoscan	terrestrial	3.1	10	-	-	-	-	-	-	-
61	Stöcker et al.	2015	gully erosion	APER0 + MicMac	terrestrial + UAV	2 + 15	35	-	-	-	-	-	-	-
62	Ryan et al.	2015	glacier drainage observation	Photoscan	UAV	500	5000	-	-	-	-	-	-	-
63	Torres-Sánchez et al.	2015	tree plantation	Photoscan	UAV	50, 100	-	-	-	-	-	-	-	-
64	Turner et al.	2015	landslide monitoring	Bundler + PMVS2	UAV	50	-	-	-	-	-	-	-	-
65	Vasuki et al.	2014	structural geology	Bundler + PMVS2	UAV	30 - 40	100	-	-	-	-	-	-	-

914

915 **These studies are considered for performance analysis.**

916 *For most authors not all camera parameters are given. Hence, camera parameters are retrieved from dpreview.com (or similar sources).*

917 * If scale or distance is not given, they are estimated from study area display.

918 **Acknowledgements**

919 The authors A. Eltner, A. Kaiser and F. Neugirg are funded by the German Research
920 Foundation (DFG) (MA 2504/15-1, HA5740/3-1, SCHM1373/8-1). A. Abellan acknowledges
921 support by the Risk Analysis group (Univ. Lausanne) and the UPC (RockRisk research
922 project BIA2013-42582-P).

923 We would like to thank an anonymous referee and Matt Westoby for their remarks, which
924 significantly improved the manuscript.

925

926 **References**

927 Abellán, A., Jaboyedoff, M., Oppikofer, T. and Vilaplana, J. M.: Detection of millimetric
928 deformation using a terrestrial laser scanner: experiment and application to a rockfall event,
929 *Nat. Hazard Earth Sys.*, 9, 365–372, 2009.

930 Abellán, A., Calvet, J., Vilaplana, J. M. and Blanchard, J.: Detection and spatial prediction of
931 rockfalls by means of terrestrial laser scanner monitoring, *Geomorphology*, 119, 162–171,
932 doi:10.1016/j.geomorph.2010.03.016, 2010.

933 Abellán, A., Oppikofer, T., Jaboyedoff, M., Rosser, N. J., Lim, M. and Lato, M. J.: Terrestrial
934 laser scanning of rock slope instabilities, *Earth Surf. Proc. Landf.*, 39(1), 80–97.
935 doi:10.1002/esp.3493, 2014.

936 Ai, M., Hu, Q., Li, J., Wang, M., Yuan, H. and Wang, S.: A Robust Photogrammetric
937 Processing Method of Low-Altitude UAV Images, *Remote Sensing*, 7, 2302–2333,
938 doi:10.3390/rs70302302, 2015.

939 Astre, H.: SfMtoolkit. <http://www.visual-experiments.com/demos/sfmtoolkit/>, last access
940 Nov. 2015.

941 Bemis, S. P., Micklethwaite, S., Turner, D., James, M. R., Akciz, S., Thiele, S. T. and
942 Bangash, H. A.: Ground-based and UAV-Based photogrammetry: A multi-scale, high-
943 resolution mapping tool for structural geology and paleoseismology, *J. Struct. Geol.*, 69, 163–
944 178, doi:10.1016/j.jsg.2014.10.007, 2014.

945 Bendig, J., Bolten, A. and Bareth, G.: UAV-based Imaging for Multi-Temporal, very high
946 Resolution Crop Surface Models to monitor Crop Growth Variability, *Photogramm.*
947 *Fernerkun.*, 6, 551–562, doi:10.1127/1432-8364/2013/02001, 2013.

948 Bini, M., Isola, I., Pappalardo, M., Ribolini, A., Favalli, M., Ragaini, L. and Zanchetta, G.:
949 Abrasive notches along the Atlantic Patagonian coast and their potential use as sea level
950 markers: the case of Puerto Deseado (Santa Cruz, Argentina), *Earth Surf. Proc. Landf.*, 39,
951 1550–1558, doi:10.1002/esp.3612, 2014.

952 Bracken, L. J., Turnbull, L., Wainwright, J. and Bogaart, P.: State of Science Sediment
953 connectivity: a framework for understanding sediment transfer at multiple scales, *Earth Surf.*
954 *Proc. Landf.*, 40, 177–188, doi:10.1002/esp.3635, 2015.

955 Brasington, J., Vericat, D. and Rychkov, I.: Modeling river bed morphology, roughness, and
956 surface sedimentology using high resolution terrestrial laser scanning, *Water Resources*
957 *Research*, 48, W11519, doi:10.1029/2012WR012223, 2012.

958 Bretar, F., Arab-Sedze, M., Champion, J., Pierrot-Deseilligny, M., Heggy, E. and
959 Jacquemoud, S.: An advanced photogrammetric method to measure surface roughness:
960 Application to volcanic terrains in the Piton de la Fournaise, Reunion Island, *Remote Sens.*
961 *Environ.*, 135, 1–11, doi:10.1016/j.rse.2013.03.026, 2013.

962 Brothelande, E., Lénat, J.-F., Normier, A., Bacri, C., Peltier, A., Paris, R., Kelfoun, K., Merle,
963 O., Finizola, A. And Garaebiti, E.: Insights into the evolution of the Yenkahe resurgent dome
964 (Siwi caldera, Tanna Island, Vanuatu) inferred from aerial high-resolution photogrammetry, *J.*
965 *Volcanol. Geoth. Res.*, doi:10.1016/j.jvolgeores.2015.04.006, 2015.

966 Brown, M. Z., Burschka, D. and Hager, G. D.: Advances in Computational Stereo, in: *IEEE*
967 *Transactions on pattern analysis and machine intelligence*, 25, 993–1008, 2003.

968 Buckley, S., Howell, J., Enge, H. and Kurz, T.: Terrestrial laser scanning in geology: data
969 acquisition, processing and accuracy considerations, *J. Geol. Soc. London*, 165, 625–638,
970 2008.

971 Burns, J. H. R., Delparte, D., Gates, R. D. and Takabayashi, M.: Integrating structure-from-
972 motion photogrammetry with geospatial software as a novel technique for quantifying 3D
973 ecological characteristics of coral reefs, *PeerJ*, 3, doi:10.7717/peerj.1077, 2015.

974 Castillo, C., Pérez, R., James, M. R., Quinton, J. N., Taguas, E. V. and Gómez, J. A.:
975 Comparing the Accuracy of Several Field Methods for Measuring Gully Erosion, *Soil Sci.*
976 *Soc. Am. J.*, 76, doi:10.2136/sssaj2011.0390, 2012.

977 Castillo, C., Taguas, E. V., Zarco-Tejada, P., James, M. R. and Gómez, J. A.: The normalized
978 topographic method: an automated procedure for gully mapping using GIS, *Earth Surf. Proc.*
979 *Landf.*, 39, 2002–2015, doi:10.1002/esp.3595, 2014.

980 Castillo, C., James, M. R., Redel-Macías, M. D., Pérez, R. and Gómez, J. A.: SF3M software:
981 3-D photo-reconstruction for non-expert users and its application to a gully network, *SOIL*, 1,
982 583–594, doi:10.5194/soil-1-583-2015, 2015.

983 Cavalli, M., Tarolli, P., Marchi, L. and Fontana, G. D.: The effectiveness of airborne LiDAR
984 data in the recognition of channel-bed morphology, *Catena*, 73(3), 249–260,
985 doi:10.1016/j.catena.2007.11.001, 2008.

986 Chandler, J.: Effective application of automated digital photogrammetry for
987 geomorphological research, *Earth Surf. Proc. Landf.*, 24, 51–63, 1999.

988 Chen, L. C., Lo, C. Y., Liu, C. L. And Chen, A. J.: Orientation modelling by matching image
989 templates of a GCP database, *Proc. 21st ACRS*, 21(2), 2000.

990 Cignoni, P., Callieri, M., Corsini, M., Dellepiane, M., Ganovelli, F. And Ranzuglia, G.:
991 MeshLab: an Open-Source Mesh Processing Tool, in: *Eurographics Italian Chapter*
992 *Conference*, Salerno, Italy, 129–136, 2008.

993 Clapuyt, F., Vanacker, V. and Van Oost, K.: Reproducibility of UAV-based earth topography
994 reconstructions based on Structure-from-Motion algorithms, *Geomorphology*,
995 doi:10.1016/j.geomorph.2015.05.011, 2015.

996 Collier, P.: The impact on topographic mapping of developments in land and air survey:
997 1900-1939, *Cartogr. Geogr. Inform.*, 29(3), 155-174, 2002.

998 Dall’Asta, E., Delaloye, R., Diotri, F., Forlani, G., Fornari, Morro di Cella, U. M.,
999 Pogliotti, P., Roncella, R. and Santise, M.: Use of UAS in a High Mountain Landscape: the
1000 Case of Gran Sommetta Rock Glacier (AO). *ISPRS – Int. Arch. Photogramm. Rem. Sens.*,
1001 XL-3/W3, 391-397, 2015.

1002 Dandois, J. P. and Ellis, E. C.: High spatial resolution three-dimensional mapping of
1003 vegetation spectral dynamics using computer vision, *Remote Sens. Environ.*, 136, 259–276,
1004 doi:10.1016/j.rse.2013.04.005, 2013.

1005 Díaz-Varela, R., de la Rosa, R., León, L. and Zarco-Tejada, P.: High-Resolution Airborne
1006 UAV Imagery to Assess Olive Tree Crown Parameters Using 3D Photo Reconstruction:
1007 Application in Breeding Trials, *Remote Sensing*, 7, 4213–4232. doi:10.3390/rs70404213,
1008 2015.

1009 Dietrich, J. T.: Riverscape Mapping with Helicopter-Based Structure-From-Motion
1010 Photogrammetry, *Geomorphology*, 252, 144–157, doi:10.1016/j.geomorph.2015.05.008,
1011 2016.

1012 Doyle, F.: The Historical Development of Analytical Photogrammetry. *Photogrammetric*
1013 *Engineering*, 15(2), 259-265, 1964.

1014 Ducher, G.: Photogrammetry - The largest operational application of remote sensing,
1015 *Photogrammetria*, 41(2), 72-82., 1987.

1016 East, A. E., Pess, G. R., Bountry, J. A., Magirl, C. S., Ritchie, A. C., Logan, J. B., Randle, T.
1017 J., Mastin, M. C., Minear, J. T., Duda, J. J., Liermann, M. C., McHenry, M. L., Beechie, T. J.
1018 and Shafroth, P. B.: Reprint of: Large-scale dam removal on the Elwha River, Washington,
1019 USA: River channel and floodplain geomorphic change, *Geomorphology*, 246, 687–708,
1020 doi:10.1016/j.geomorph.2015.04.027, 2015.

1021 Eling, C., Wieland, M., Hess, C., Klingbeil, L. and Kuhlmann, H.: Development and
1022 evaluation of a UAV based mapping system for remote sensing and surveying applications,
1023 *ISPRS – Int. Arch. Photogramm. Rem. Sens.*, XL-1/W4, 233-239, 2015.

1024 Eltner, A., Mulsow, C. and Maas, H.: Quantitative Measurement of Soil Erosion from Tls and
1025 Uav Data, *ISPRS - Int. Arch. Photogramm. Rem. Sens.*, XL-1/W2, 119–124, 2013.

1026 Eltner, A. and Baumgart, P.: Accuracy constraints of terrestrial Lidar data for soil erosion
1027 measurement: Application to a Mediterranean field plot, *Geomorphology*, 245, 243–254,
1028 doi:10.1016/j.geomorph.2015.06.008, 2015.

1029 Eltner, A., Baumgart, P., Maas, H.-G. and Faust, D.: Multi-temporal UAV data for automatic
1030 measurement of rill and interrill erosion on loess soil. *Earth Surf. Proc. Landf.*, 40(6), 741–
1031 755, doi:10.1002/esp.3673, 2015.

1032 Eltner, A. and Schneider, D.: Analysis of Different Methods for 3D Reconstruction of Natural
1033 Surfaces from Parallel-Axes UAV Images, *Photogramm. Rec.*, 30(151), 279–299,
1034 doi:10.1111/phor.12115, 2015.

1035 Favalli, M., Fornaciai, A., Isola, I., Tarquini, S. and Nannipieri, L.: Multiview 3D
1036 reconstruction in geosciences, *Comput. Geosc.*, 44, 168–176,
1037 doi:10.1016/j.cageo.2011.09.012, 2012.

- 1038 Fekete, S., Diederichs, M. and Lato, M.: Geotechnical and operational applications for 3-
1039 dimensional laser scanning in drill and blast tunnels, *Tunnelling and Underground Space*
1040 *Technology*, 25(5), 614–628, doi:10.1016/j.tust.2010.04.008, 2010.
- 1041 Fernández, T., Pérez, J. L., Cardenal, F. J., López, A., Gómez, J. M., Colomo, C., Delgado, J.
1042 and Sánchez, M.: Use of a Light UAV and Photogrammetric Techniques To Study the
1043 Evolution of a Landslide in Jaén (Southern Spain), *ISPRS – Int. Arch. Photogramm. Rem.*
1044 *Sens.*, XL-3/W3, 241–248, doi:10.5194/isprsarchives-XL-3-W3-241-2015, 2015.
- 1045 Fonstad, M. A., Dietrich, J. T., Courville, B. C., Jensen, J. L. and Carbonneau, P. E.:
1046 Topographic structure from motion: a new development in photogrammetric measurement,
1047 *Earth Surf. Proc. Landf.*, 38, 421–430, doi:10.1002/esp.3366, 2013.
- 1048 Frahm, J.-M., Pollefeys, M., Lazebnik, S., Gallup, D., Clipp, B., Raguram, R., Wu, C., Zach,
1049 C. and Johnson, T.: Fast robust large-scale mapping from video and internet photo
1050 collections., *ISPRS J. Photogramm.*, 65(6), 538–549, doi:10.1016/j.isprsjprs.2010.08.009,
1051 2010.
- 1052 Franceschi, M., Teza, G., Preto, N., Pesci, A., Galgaro, A. and Girardi, S.: Discrimination
1053 between marls and limestones using intensity data from terrestrial laser scanner, *ISPRS J.*
1054 *Photogramm.*, 64(6), 522–528, doi:10.1016/j.isprsjprs.2009.03.003, 2009.
- 1055 Francioni, M., Salvini, R., Stead, D., Giovannini, R., Riccucci, S., Vanneschi, C. and Gulli,
1056 D.: An integrated remote sensing-GIS approach for the analysis of an open pit in the Carrara
1057 marble district, Italy: Slope stability assessment through kinematic and numerical methods,
1058 *Comp. Geot.*, 67, 46–63, doi:10.1016/j.compgeo.2015.02.009, 2015.
- 1059 Frankl, A., Stal, C., Abraha, A., Nyssen, J., Rieke-Zapp, D., De Wulf, A. and Poesen, J.:
1060 Detailed recording of gully morphology in 3D through image-based modelling PhotoScan
1061 Digital Elevation Model (DEM) Soil pipes Structure from Motion–Multi View Stereo
1062 (SfM–MVS) Volume calculation, *Catena*, 127, 92–101, doi:10.1016/j.catena.2014.12.016,
1063 2014.
- 1064 Fugazza, D., Senese, A., Azzoni, R. S., Smiraglia, C. Cernuschi, M. Severi, D. D. and
1065 Guglielmina, A.: High-resolution mapping of glacier surface features. The UAV survey of the
1066 Forni glacier (Stelvio National Park, Italy), *Geogr. Fis. Dinam. Quat.*, 38, 25-33,
1067 doi:10.4461/GFDQ.2015.38.03, 2015.

1068 Furukawa, Y., Curless, B., Seitz, S. M. and Szeliski, R.: Towards Internet-scale multi-view
1069 stereo, in: IEEE Conference on Computer Vision and Pattern Recognition, San Francisco,
1070 CA, USA, 1434–1441, doi:10.1109/CVPR.2010.5539802, 2010.

1071 Furukawa, Y. and Ponce, J.: Accurate, dense, and robust multiview stereopsis, in: IEEE
1072 Transactions on Pattern Analysis and Machine Intelligence, 83, 1362–1376,
1073 doi:10.1109/TPAMI.2009.161, 2010.

1074 Genchi, S. A., Vitale, A. J., Perillo, G. M. E. and Delrieux, C. A.: Structure-from-Motion
1075 Approach for Characterization of Bioerosion Patterns Using UAV Imagery, Sensors, 15,
1076 3593–3609, doi:10.3390/s150203593, 2015.

1077 Gienko, G. A. and Terry, J. P.: Three-dimensional modeling of coastal boulders using multi-
1078 view image measurements, Earth Surf. Proc. Landf., 39, 853–864, doi:10.1002/esp.3485,
1079 2014.

1080 Gigli, G. and Casagli, N.: Semi-automatic extraction of rock mass structural data from high
1081 resolution LIDAR point clouds., Int. J. Rock Mech. Min., 48, 187–198,
1082 doi:10.1016/j.ijrmms.2010.11.009, 2011.

1083 Girardeau-Montaut, D.: CloudCompare (version 2.x; GPL software), EDF RandD, Telecom
1084 ParisTech, <http://www.cloudcompare.org/>, last access: Mar. 2015.

1085 Gomez, C.: Digital photogrammetry and GIS-based analysis of the bio-geomorphological
1086 evolution of Sakurajima Volcano, diachronic analysis from 1947 to 2006. J. Volcanol. Geoth.,
1087 280, 1–13, 2014.

1088 Gomez, C., Hayakawa, Y. and Obanawa, H.: A study of Japanese landscapes using structure
1089 from motion derived DSMs and DEMs based on historical aerial photographs: New opportu-
1090 nities for vegetation monitoring and diachronic geomorphology, Geomorphology, 242, 11–20,
1091 doi:10.1016/j.geomorph.2015.02.021, 2015.

1092 Gómez-Gutiérrez, Á., de Sanjosé-Blasco, J. J., de Matías-Bejarano, J. and Berenguer-
1093 Sempere, F.: Comparing Two Photo-Reconstruction Methods to Produce High Density Point
1094 Clouds and DEMs in the Corral del Veleta Rock Glacier (Sierra Nevada, Spain), Remote
1095 Sensing, 6, 5407–5427, doi:10.3390/rs6065407, 2014.

1096 Gómez-Gutiérrez, Á., Schnabel, S., Berenguer-Sempere, F., Lavado-Contador, F. and Rubio-
1097 Delgado, J.: Using 3D photo-reconstruction methods to estimate gully headcut erosion,
1098 Catena, 120, 91–101, doi:10.1016/j.catena.2014.04.004, 2014.

1099 Gómez-Gutiérrez, Á., de Sanjosé-Blasco, J., Lozano-Parra, J., Berenguer-Sempere, F. and de
1100 Matías-Bejarano, J.: Does HDR Pre-Processing Improve the Accuracy of 3D Models
1101 Obtained by Means of two Conventional SfM-MVS Software Packages? The Case of the
1102 Corral del Veleta Rock Glacier, *Remote Sensing*, 7, 10269–10294, doi:10.3390/rs70810269,
1103 2015.

1104 Gruen, A.: Development and status of image matching in photogrammetry, *Photogramm.*
1105 *Rec.*, 27(137), 36–57, doi:10.1111/j.1477-9730.2011.00671.x, 2012.

1106 Hartzell, P., Glennie, C., Biber, K., and Khan, S. (2014). Application of multispectral LiDAR
1107 to automated virtual outcrop geology. *ISPRS Journal of Photogrammetry and Remote*
1108 *Sensing*, 88, 147–155. doi:10.1016/j.isprsjprs.2013.12.004

1109 Harwin, S. and Lucieer, A.: Assessing the Accuracy of Georeferenced Point Clouds Produced
1110 via Multi-View Stereopsis from Unmanned Aerial Vehicle (UAV) Imagery, *Remote Sensing*,
1111 4, 1573–1599, doi:10.3390/rs4061573, 2012.

1112 Heritage, G. and Hetherington, D.: Towards a protocol for laser scanning in fluvial
1113 geomorphology, *Earth Surf. Proc. Landf.*, 32(32), 66–74, doi:10.1002/esp.1375, 2007.

1114 Hirschmüller, H.: Semi-Global Matching – Motivation, Developments and Applications,
1115 *Photogrammetric Week*, 11, 173–184, 2011.

1116 Humair, F., Abellan, A., Carrea, D., Matasci, B., Epard, J.-L. and Jaboyedoff, M.: Geological
1117 layers detection and characterisation using high resolution 3D point clouds: example of a box-
1118 fold in the Swiss Jura Mountains, *Eur. J. Rem. Sens.*, 48, 541–568,
1119 doi:10.5721/EuJRS20154831, 2015.

1120 Immerzeel, W. W., Kraaijenbrink, A., Shea, J. M., Shrestha, A. B., Pellicciotti, F., Bierkens,
1121 M. F. P. and De Jong, S. M.: High-resolution monitoring of Himalayan glacier dynamics
1122 using unmanned aerial vehicles, *Rem. Sens. Environ.*, 150, 93–103,
1123 doi:10.1016/j.rse.2014.04.025, 2014.

1124 Jaboyedoff, M., Metzger, R., Oppikofer, T., Couture, R., Derron, M.-H., Locat, J. and Turmel,
1125 D.: New insight techniques to analyze rock-slope relief using DEM and 3D- imaging cloud
1126 points: COLTOP-3D software. In: *Rock Mechanics: Meeting Society's Challenges and*
1127 *Demands*, Eberhardt, E., Stead, D. and Morrison, T. (Eds.), 1st ed., Taylor and Francis,
1128 London, 61–68, 2007.

1129 Jaboyedoff, M., Oppikofer, T., Abellán, A., Derron, M.-H., Loye, A., Metzger, R. and
1130 Pedrazzini, A.: Use of LIDAR in landslide investigations: a review, *Nat. Hazards*, 61, 5-28,
1131 doi: 10.1007/s11069-010-9634-2, 2012.

1132 Jackson, M. and Magro, G.: Real-time crowd-sourcing, data and modelling. In: IAIA15
1133 Conference Proceedings, Florence, 2015.

1134 James, M. R. and Robson, S.: Straightforward reconstruction of 3D surfaces and topography
1135 with a camera: Accuracy and geoscience application, *J. Geoph. Res.*, 117, F03017,
1136 doi:10.1029/2011JF002289, 2012.

1137 James, M. R. and Varley, N.: Identification of structural controls in an active lava dome with
1138 high resolution DEMs: Volcán de Colima, Mexico, *Geoph. Res. Let.*, 39, L22303,
1139 doi:10.1029/2012GL054245, 2012.

1140 James, M. R. and Robson, S.: Mitigating systematic error in topographic models derived from
1141 UAV and ground-based image networks, *Earth Surf. Proc. Landf.*, 39, 1413–1420,
1142 doi:10.1002/esp.3609, 2014.

1143 James, M. R. and Robson, S.: Sequential digital elevation models of active lava flows from
1144 ground-based stereo time-lapse imagery, *ISPRS J. Photogramm. Rem. Sens.*, 97, 160–170,
1145 doi:10.1016/j.isprsjprs.2014.08.011, 2014.

1146 Javernick, L., Brasington, J. and Caruso, B.: Modeling the topography of shallow braided
1147 rivers using Structure-from-Motion photogrammetry, *Geomorphology*, 213, 166–182,
1148 doi:10.1016/j.geomorph.2014.01.006, 2014.

1149 Johnson, K., Nissen, E., Saripalli, S., Arrowsmith, J. R., McGarey, P., Scharer, K., Williams,
1150 P. and Blisniuk, K.: Rapid mapping of ultrafine fault zone topography with structure from
1151 motion, *Geosphere*, 10(5), doi:10.1130/GES01017.1, 2014.

1152 Johnson-Roberson, M., Bryson, M., Douillard, B., Pizarro, O. and Williams, S. B.:
1153 Discovering salient regions on 3D photo-textured maps: Crowdsourcing interaction data from
1154 multitouch smartphones and tablets, *Comput. Vis. Image Und.*, 131, 28–41,
1155 doi:10.1016/j.cviu.2014.07.006, 2015.

1156 Kääb, A.: Glacier Volume Changes Using ASTER Satellite Stereo and ICESat GLAS Laser
1157 Altimetry. A Test Study on Edgeøya, Eastern Svalbard, *IEEE Transactions on Geoscience
1158 and Remote Sensing*, 46(10), 2823 – 2830, doi:10.1109/TGRS.2008.2000627, 2008.

1159 Kääb, A., Girod, L. and Berthling, I.: Surface kinematics of periglacial sorted circles using
1160 structure-from-motion technology, *The Cryosphere*, 8, 1041–1056, doi:10.5194/tc-8-1041-
1161 2014, 2014.

1162 Kaiser, A., Neugirg, F., Rock, G., Müller, C., Haas, F., Ries, J., and Schmidt, J.: Small-Scale
1163 Surface Reconstruction and Volume Calculation of Soil Erosion in Complex Moroccan Gully
1164 Morphology Using Structure from Motion, *Remote Sensing*, 6, 7050–7080,
1165 doi:10.3390/rs6087050, 2014.

1166 Kaiser, A., Neugirg, F., Haas, F., Schmidt, J., Becht, M. and Schindewolf, M.: Determination
1167 of hydrological roughness by means of close range remote sensing, *SOIL*, 1, 613–620,
1168 doi:10.5194/soil-1-613-2015, 2015.

1169 Khoshelham, K., Altundag, D., Ngan-Tillard, D. and Menenti, M.: Influence of range
1170 measurement noise on roughness characterization of rock surfaces using terrestrial laser
1171 scanning, *Int. J. Rock Mech. Min.*, 48, 1215–1223, doi:10.1016/j.ijrmms.2011.09.007, 2011.

1172 Kraus, K.: *Photogrammetry: Geometry from Images and Laser Scans*, 2nd edition, De
1173 Gruyter, Berlin, Germany, 459 pages, 2007.

1174 Kromer, R., Abellán, A., Hutchinson, D., Lato, M., Edwards, T. and Jaboyedoff, M.: A 4D
1175 Filtering and Calibration Technique for Small-Scale Point Cloud Change Detection with a
1176 Terrestrial Laser Scanner, *Remote Sensing*, 7(10), 13029–13052, doi:10.3390/rs71013029,
1177 2015.

1178 Lague, D., Brodu, N., and Leroux, J.: Accurate 3D comparison of complex topography with
1179 terrestrial laser scanner: Application to the Rangitikei canyon (N-Z), *ISPRS J. Photogramm.*
1180 *Rem. Sens.*, 82, 10–26, doi:10.1016/j.isprsjprs.2013.04.009, 2013.

1181 Laussedat, A.: *La métrophotographie*, Bibliothèque Photographique, Gauthier-Villars, Paris,
1182 55 pages, 1899.

1183 Lato, M., Hutchinson, J., Diederichs, M., Ball, D. and Harrap, R.: Engineering monitoring of
1184 rockfall hazards along transportation corridors: using mobile terrestrial LiDAR, *Nat. Hazard*
1185 *Earth Sys.*, 9, 935–946, 2009.

1186 Leon, J. X., Roelfsema, C. M., Saunders, M. I. and Phinn, S. R.: Measuring coral reef terrain
1187 roughness using “Structure-from-Motion” close-range photogrammetry, *Geomorphology*,
1188 242, 21–28, doi:10.1016/j.geomorph.2015.01.030, 2015.

1189 Lim, M., Petley, D. N., Rosser, N. J., Allison, R. J., Long, A. J. and Pybus, D.: Combined
1190 digital photogrammetry and time-of-flight laser scanning for monitoring cliff evolution,
1191 *Photogramm. Rec.*, 20(110), 109–129, 2008.

1192 Lowe, D. G.: Object recognition from local scale-invariant features, *The Proceedings of the*
1193 *7th IEEE International Conference on Computer Vision*, 2, 1150–1157, 1999.

1194 Lucieer, A., de Jong, S. and Turner, D.: Mapping landslide displacements using Structure
1195 from Motion (SfM) and image correlation of multi-temporal UAV photography, *Prog. Phys.*
1196 *Geog.*, 38, 1–20, doi:10.1177/0309133313515293, 2013.

1197 Lucieer, A., Turner, D., King, D. H. and Robinson, S. A.: Using an unmanned aerial vehicle
1198 (UAV) to capture micro-topography of antarctic moss beds, *Int. J. Appl. Earth Obs.*, 27, 53–
1199 62, doi:10.1016/j.jag.2013.05.011, 2014.

1200 Luhmann, T., Robson, S., Kyle, S. and Boehm, J.: *Close-Range Photogrammetry and 3D*
1201 *Imaging*, 2nd edition, De Gruyter, Berlin, Germany, 683 pages, 2014.

1202 Mancini, F., Dubbini, M., Gattelli, M., Stecchi, F., Fabbri, S. and Gabbianelli, G.: Using
1203 Unmanned Aerial Vehicles (UAV) for High-Resolution Reconstruction of Topography: The
1204 Structure from Motion Approach on Coastal Environments, *Remote Sensing*, 5, 6880–6898,
1205 doi:10.3390/rs5126880, 2013.

1206 Martin-Brualla, R., Gallup, D. and Seitz, S. M.: Time-lapse Mining from Internet Photos. in:
1207 *IEEE International Conference on Computer Vision (ICCV)*, 2015.

1208 Masiero, A., Guarnieri, A., Vettore, A. and Pirotti, F.: An ISVD-based Euclidian structure
1209 from motion for smartphones, *Int. Arch. Photogramm. Rem. Sens.*, XL-5, 401-406, 2014.

1210 Meesuk, V., Vojinovic, Z., Mynett, A. E., and Abdullah, A. F.: Urban flood modelling
1211 combining top-view LiDAR data with ground-view SfM observations, *Adv. Water Res.*, 75,
1212 105–117, doi:10.1016/j.advwatres.2014.11.008, 2015.

1213 Micheletti, N., Chandler, J. H. and Lane, S. N.: Investigating the geomorphological potential
1214 of freely available and accessible structure-from-motion photogrammetry using a smartphone,
1215 *Earth Surf. Proc. Landf.*, 40, 473–486, doi:10.1002/esp.3648, 2014.

1216 Micheletti, N., Chandler, J. H. and Lane, S. N.: Structure from Motion (SfM)
1217 Photogrammetry (Chap. 2, Sec. 2.2), In: Cook, S.J., Clarke L.E. and Nield, J.M. (Eds.)
1218 *Geomorphological Techniques*, British Society of Geomorphology, London, 2015.

1219 Michoud, C., Carrea, D., Costa, S., Derron, M.-H., Jaboyedoff, M., Delacourt, C., Maquaire,
1220 O., Letortu, P. and Davidson, R.: Landslide detection and monitoring capability of boat-based
1221 mobile laser scanning along Dieppe coastal cliffs, Normandy, *Landslides*, 12(2), 403–418,
1222 2015.

1223 Mikhail, E., Bethel, J. and McGlone, J.: *Introduction to Modern Photogrammetry*, John Wiley
1224 and Sons, Inc., New York, 479 pages, 2001.

1225 Milan, D. J., Heritage, G. L. and Hetherington, D.: Assessment of erosion and deposition
1226 volumes and channel change Application of a 3D laser scanner in the assessment of erosion
1227 and deposition volumes and channel change in a proglacial river, *Earth Surf. Proc. Landf.*,
1228 32(32), 1657–1674, doi:10.1002/esp.1592, 2007.

1229 Monserrat, O. and Crosetto, M.: Deformation measurement using terrestrial laser scanning
1230 data and least squares 3D surface matching, *ISPRS J. Photogramm. Rem. Sens.*, 63(1), 142–
1231 154, doi:10.1016/j.isprsjprs.2007.07.008, 2008.

1232 Morgenroth, J. and Gomez, C.: Assessment of tree structure using a 3D image analysis
1233 technique—A proof of concept; *Urban Forestry and Urban Greening*, 13(1), 198–203,
1234 doi:10.1016/j.ufug.2013.10.005, 2014

1235 Nadal-Romero, E., Revuelto, J., Errea, P. and López-Moreno, J. I.: The application of
1236 terrestrial laser scanner and SfM photogrammetry in measuring erosion and deposition
1237 processes in two opposite slopes in a humid badlands area (central Spanish Pyrenees), *SOIL*,
1238 1, 561–573, doi:10.5194/soil-1-561-2015, 2015.

1239 Nolan, M., Larsen, C. and Sturm, M.: Mapping snow-depth from manned-aircraft on
1240 landscape scales at centimeter resolution using Structure-from-Motion photogrammetry, *The*
1241 *Cryosphere Disc.*, 9, 333–381, doi:10.5194/tcd-9-333-2015, 2015.

1242 Nouwakpo, S. K., James, M. R., Wertz, M. A., Huang, C.-H., Chagas, I. and Lima, L.:
1243 Evaluation of structure from motion for soil microtopography measurement, *Photogramm.*
1244 *Rec.*, 29(147), 297–316, doi:10.1111/phor.12072, 2014.

1245 Nouwakpo, S. K., Wertz, M. A. and McGwire, K.: Assessing the performance of Structure-
1246 from-Motion photogrammetry and terrestrial lidar for reconstructing soil surface
1247 microtopography of naturally vegetated plots, *Earth Surf. Proc. Landf.*, doi:10.1002/esp.3787,
1248 2015.

- 1249 Oppikofer, T., Jaboyedoff, M., Blikra, L., Derron, M.-H. and Metzger, R.: Characterization
1250 and monitoring of the Aknes rockslide using terrestrial laser scanning, *Natural Hazards and*
1251 *Earth System Sciences*, 9, 1003–1019, 2009.
- 1252 Ouédraogo, M. M., Degré, A., Debouche, C. and Lisein, J.: The evaluation of unmanned
1253 aerial system-based photogrammetry and terrestrial laser scanning to generate DEMs of
1254 agricultural watersheds, *Geomorphology*, 214, 339–355,
1255 doi:10.1016/j.geomorph.2014.02.016, 2014.
- 1256 Passalacqua, P., Belmont, P., Staley, D. M., Simley, J. D., Arrowsmith, J. R., Bode, C. A.,
1257 Crosby, C., DeLong, S. B., Glenn, N. F., Kelly, S. A., Lague, D., Sangireddy, H., Schaffrath,
1258 K., Tarboton, D. G., Wasklewicz, T. and Wheaton, J. M.: Analyzing high resolution
1259 topography for advancing the understanding of mass and energy transfer through landscapes:
1260 A review. *Earth-Sci. Rev.*, 148, 174–193, doi:10.1016/j.earscirev.2015.05.012, 2015.
- 1261 Pears, N., Liu, Y. and Bunting, P.: *3D Imaging, Analysis and Applications*, Springer, London,
1262 499 pages, 2012.
- 1263 Piermattei, L., Carturan, L. and Guarnieri, A.: Use of terrestrial photogrammetry based on
1264 structure from motion for mass balance estimation of a small glacier in the Italian Alps, *Earth*
1265 *Surf. Proc. Landf.*, 40(13), 1791–1802, doi:10.1002/esp.3756, 2015.
- 1266 Pierrot-Deseilligny, M. and Clery, I.: APERO, an open source bundle adjustment software for
1267 automatic calibration and orientation of set of images, *Intern. Arch. Photogramm. Rem. Sens.*,
1268 38-5(W16), 269–276, 2011.
- 1269 Pierrot-Deseilligny, M. and Clery, I.: Some possible protocols of acquisition for the optimal
1270 use of the “Apero” open source software in automatic orientation and calibration, *EuroCow*
1271 2012, Barcelona, Spain, (10pp), 2012.
- 1272 Pike, R. J., Evans, I. S. and Hengl, T.: Geomorphometry: a Brief Guide. In: Hengl, T. and
1273 Reuter, H.I. (Eds) *Geomorphometry: Concepts, Software, Applications*. *Developments in Soil*
1274 *Science*, 33, 1-28, 2008.
- 1275 Pollyea, R. and Fairley, J.: Estimating surface roughness of terrestrial laser scan data using
1276 orthogonal distance regression, *Geology*, 39(7), 623–626, doi:10.1130/G32078.1, 2011.
- 1277 Poropat, G.: Measurement of Surface Roughness of Rock Discontinuities. In *Proc. of the 3rd*
1278 *CANUS Rock Mechanics Symposium*. Toronto, 2009.

- 1279 Prosdocimi, M., Calligaro, S., Sofia, G., Dalla Fontana, G. and Tarolli, P.: Bank erosion in
1280 agricultural drainage networks: new challenges from Structure-from-Motion photogrammetry
1281 for post-event analysis, *Earth Surf. Proc. Landf.*, 40(14), 1891–1906, doi:10.1002/esp.3767,
1282 2015.
- 1283 Remondino, F., Spera, M. G., Nocerino, E., Menna, F. and Nex, F.: State of the art in high
1284 density image matching, *Photogramm. Rec.*, 29(146), 144–166, doi:10.1111/phor.12063,
1285 2014.
- 1286 Rippin, D. M., Pomfret, A. and King, N.: High resolution mapping of supraglacial drainage
1287 pathways reveals link between micro-channel drainage density, surface roughness and surface
1288 reflectance, *Earth Surf. Proc. Landf.*, 40(10), 1279–1290, doi:10.1002/esp.3719, 2015.
- 1289 Royan, M., Abellan, A. and Vilaplana, J.: Progressive failure leading to the 3 December 2013
1290 rockfall at Puigcercós scarp (Catalonia, Spain), *Landslides*, 12(3), 585–595, 2015.
- 1291 Ruzic, I., Marovic, I., Benac, C. and Ilic, S.: Coastal cliff geometry derived from structure-
1292 from-motion photogrammetry at Stara Baka, Krk Island, Croatia, *Geo-Mar. Lett.*, 34, 555–
1293 565, doi:10.1007/s00367-014-0380-4, 2014.
- 1294 Ryan, J. C., Hubbard, A. L., Box, J. E., Todd, J., Christoffersen, P., Carr, J. R., Holt, T. O.,
1295 and Snooke, N.: UAV photogrammetry and structure from motion to assess calving dynamics
1296 at Store Glacier, a large outlet draining the Greenland ice sheet, *The Cryosphere*, 9, 1-11,
1297 doi:10.5194/tc-9-1-2015, 2015.
- 1298 Sanz-Ablanedo, E., Rodríguez-Pérez, J. R., Armesto, J. and Taboada, M. F. Á.: Geometric
1299 stability and lens decentering in compact digital cameras, *Sensors*, 10, 1553–1572
1300 doi:10.3390/s100301553, 2010.
- 1301 Schaffalitzky, F. and Zisserman, A.: Multi-view matching for unordered image sets, or “How
1302 do I organize my holiday snaps?”, *Computer Vision - ECCV 2002*, 2350, 414–431.
1303 doi:10.1007/3-540-47969-4, 2002.
- 1304 Shortis, M. R., Bellman, C. J., Robson, S., Johnston, G. J. and Johnson, G. W.: Stability of
1305 Zoom and Fixed Lenses used with Digital SLR Cameras, *Intern. Arch. Photogramm., Rem.*
1306 *Sens.*, XXXVI(5), 285–290, 2006.
- 1307 Siebert, S. and Teizer, J.: Mobile 3D mapping for surveying earthwork projects using an
1308 Unmanned Aerial Vehicle (UAV) system, *Automation in Construction*, 41, 1–14,
1309 doi:10.1016/j.autcon.2014.01.004, 2014.

1310 Smith, M. W., Carrivick, J. L., Hooke, J. and Kirkby, M. J.: Reconstructing flash flood
1311 magnitudes using “Structure-from-Motion”: A rapid assessment tool, *J. Hydrol.*, 519, 1914–
1312 1927, doi:10.1016/j.jhydrol.2014.09.078, 2014.

1313 Smith, M. W. and Vericat, D.: From experimental plots to experimental landscapes:
1314 topography, erosion and deposition in sub-humid badlands from Structure-from-Motion
1315 photogrammetry, *Earth Surf. Proc. Landf.*, 40(12), 1656–1671, doi:10.1002/esp.3747, 2015.

1316 Smith, M. W., Carrivick, J. L. and Quincey, D. J.: Structure from motion photogrammetry in
1317 physical geography, *Progress in Physical Geography*, 1-29, doi: 10.1177/0309133315615805,
1318 2015.

1319 Snapir, B., Hobbs, S. and Waine, T. W.: Roughness measurements over an agricultural soil
1320 surface with Structure from Motion, *ISPRS J. Photogramm. Rem. Sens.*, 96, 210–223,
1321 doi:10.1016/j.isprsjprs.2014.07.010, 2014.

1322 Snavely, N., Seitz, S. M. and Szeliski, R.: Photo Tourism : Exploring Photo Collections in 3D,
1323 *ACM Transactions on Graphics*, 25(3), 835–846, 2006.

1324 Snavely, N., Seitz, S. M. and Szeliski, R.: Modeling the World from Internet Photo
1325 Collections, *Intern. J. Comput. Vis.*, 80(2), 189–210. doi:10.1007/s11263-007-0107-3, 2008.

1326 Stöcker, C., Eltner, A. and Karrasch, P.: Measuring gullies by synergetic application of UAV
1327 and close range photogrammetry — A case study from Andalusia, Spain, *Catena*, 132, 1–11,
1328 doi:10.1016/j.catena.2015.04.004, 2015.

1329 Stumpf, A., Malet, J.-P., Allemand, P., Pierrot-Deseilligny, M. and Skupinski, G.: Ground-
1330 based multi-view photogrammetry for the monitoring of landslide deformation and erosion,
1331 *Geomorphology*, 231, 130–145, doi:10.1016/j.geomorph.2014.10.039, 2014.

1332 Sturzenegger, M. and Stead, D.: Close-range terrestrial digital photogrammetry and terrestrial
1333 laser scanning for discontinuity characterization on rock cuts, *Eng. Geol.*, 106, 163–182,
1334 doi:10.1016/j.enggeo.2009.03.004, 2009.

1335 Tamminga, A. D., Eaton, B. C. and Hugenholtz, C. H.: UAS-based remote sensing of Wuvial
1336 change following an extreme Wood event, *Earth Surf. Proc. Landf.*, 40(11), 1464–1476,
1337 doi:10.1002/esp.3728, 2015.

1338 Thomsen, L., Stolte, J., Baartman, J. and Starkloff, T.: Soil roughness : comparing old and
1339 new methods and application in a soil erosion model, *SOIL*, 1, 399–410, doi:10.5194/soil-1-
1340 399-2015, 2015.

1341 Tonkin, T. N., Midgley, N. G., Graham, D. J. and Labadz, J. C.: The potential of small
1342 unmanned aircraft systems and structure-from-motion for topographic surveys: A test of
1343 emerging integrated approaches at Cwm Idwal, North Wales, *Geomorphology*, 226, 35–43,
1344 doi:10.1016/j.geomorph.2014.07.021, 2014.

1345 Torres-Sánchez, J., López-Granados, F., Serrano, N., Arquero, O. and Peña, J. M.: High-
1346 Throughput 3-D Monitoring of Agricultural-Tree Plantations with Unmanned Aerial Vehicle
1347 (UAV) Technology, *PLOS One*, 10(6), doi:10.1371/journal.pone.0130479, 2015.

1348 Triggs, B., McLauchlan, P., Hartley, R. and Fitzgibbon, A.: Bundle Adjustment - A Modern
1349 Synthesis. In: Triggs, B., Zisserman, A. and Szeliski, R. (Eds.), *Vision Algorithms: Theory
1350 and Practice*, Springer, Berlin, Germany, LNCS vol. 1883, 298–372, 2000.

1351 Turner, D., Lucieer, A. and de Jong, S.: Time Series Analysis of Landslide Dynamics Using
1352 an Unmanned Aerial Vehicle (UAV), *Remote Sensing*, 7, 1736–1757,
1353 doi:10.3390/rs70201736, 2015.

1354 Ullman, S.: The interpretation of structure from motion. *Proceedings of the Royal Society B*,
1355 203, 405–426, 1979.

1356 Vasuki, Y., Holden, E. J., Kovesi, P. and Micklethwaite, S.: Semi-automatic mapping of
1357 geological Structures using UAV-based photogrammetric data: An image analysis approach,
1358 *Comput. Geosci.*, 69, 22–32, doi:10.1016/j.cageo.2014.04.012, 2014.

1359 Westoby, M. J., Brasington, J., Glasser, N. F., Hambrey, M. J. and Reynolds, J. M.:
1360 “Structure-from-Motion” photogrammetry: A low-cost, effective tool for geoscience
1361 applications, *Geomorphology*, 179, 300–314, doi:10.1016/j.geomorph.2012.08.021, 2012.

1362 Westoby, M. J., Glasser, N. F., Hambrey, M. J., Brasington, J., Reynolds, J. M. and Hassan,
1363 M. A. A. M.: Reconstructing historic glacial lakeoutburst floods through numerical modelling
1364 and geomorphological assessment: Extreme events in the Himalaya, *Earth Surf. Proc. Landf.*,
1365 39, 1675–1692, doi:10.1002/esp.3617, 2014.

1366 Woodget, A. S., Carbonneau, P. E., Visser, F. and Maddock, I. P.: Quantifying submerged
1367 fluvial topography using hyperspatial resolution UAS imagery and structure from motion
1368 photogrammetry, *Earth Surf. Proc. Landf.*, 40(1), 47–64, doi:10.1002/esp.3613, 2015.

1369 Wu, C.: Towards linear-time incremental structure from motion, in: *International Conference
1370 on 3D Vision - 3DV*, Seattle, WA, USA, 127–134, 2013.

1371 Wu, C.: Critical configurations for radial distortion self-calibration, in: IEEE Conference on
1372 Computer Vision and Pattern Recognition (CVPR), 25 – 32. doi:10.1109/CVPR.2014.11,
1373 2014.

1374 Zarco-Tejada, P. J., Diaz-Varela, R., Angileri, V. and Loudjani, P.: Tree height quantification
1375 using very high resolution imagery acquired from an unmanned aerial vehicle (UAV) and
1376 automatic 3D photo-reconstruction methods, *Eur. J. Agron.*, 55, 89–99,
1377 doi:10.1016/j.eja.2014.01.004, 2014.

1378

1379

Image-based 3D reconstruction	recording of the three-dimensional shape of an object from overlapping images from different perspectives
Computer Vision	algorithmic efforts to imitate human vision with focus on automation, amongst others, to reconstruct 3D scenes with methods of image processing and image understanding
Structure from Motion (SfM)	fully automatic reconstruction of 3D scenes from 2D images and simultaneous retrieval of the corresponding camera geometry in an arbitrary coordinate system
Photogrammetry	algorithmic efforts to determine 3D model coordinates and camera geometry focussing on accuracy and precise measurement in images
SfM photogrammetry	fully automatic reconstruction of 3D scenes from 2D images and camera geometry with option to set parameters for (photogrammetric) optimisation of accuracy and precision
Dense matching	increase of resolution of point clouds that model 3D scenes by pixel- or patch-wise matching in images of known intrinsic and extrinsic parameters
Stereo matching	reconstruction of object point through matching (in image space, Remondino et al., 2014) between two overlapping images
Multi-View-Stereo (MVS) matching	reconstruction of object point through matching (in object space, Remondino et al., 2014) from multiple overlapping images
Extrinsic parameters	exterior camera geometry comprising position (three shifts) and orientation (three rotations) of the camera projection centre
Intrinsic parameters	interior camera geometry comprising principle distance (distance between projection centre and image sensor), principle point (intersection of perpendicular from projection centre onto image plane) and distortion parameters (e.g. radial distortion)
Bundle adjustment (BA)	least-square optimisation to simultaneously solve for extrinsic (and intrinsic) parameters of all images; the term bundle correlates to rays that derive from 3D points, converge in corresponding projection centres and intersect with image sensor
Camera self-calibration	intrinsic camera parameters are included as additional unknowns into BA to solve for interior camera geometry
Ground Control Point (GCP)	in images clearly distinguishable point whose object coordinates are known to geo-reference surface model
Digital Elevation Model (DEM)	3D description of the surface in either raster (grid) or vector (mesh) format
Point cloud	quantity of points of 3D coordinates describing the surface within arbitrary or geo-referenced coordinate system, additional information such as normals or colours possible

Table 2: Summary of non-commercial software tools beneficial for SfM photogrammetry processing and post-processing.

<i>Software</i>	<i>Bundler</i>	<i>PMVS2</i>	<i>Apero+ Mac</i>	<i>SfMToolkit</i>	<i>Meshlab</i>	<i>Cloud Compare</i>	<i>Sfm_georef</i>	<i>VisualSFM</i>	<i>SF3M</i>	<i>Photosynth</i>	<i>123D Catch</i>
<i>Type</i>	Open Source	Open Source	Open Source	Open Source	Open Source	Open Source	Freely- available	Freely- available	Freely- available	Free web service	Free web service
<i>Website</i>	http://www.cs.cornell.edu/~snave/bundler	http://www.dti.ens.fr/pmvs	http://logiciel.s.ign.fr/?Micmac	http://www.visual-experiments.com/demos/sfmtoolkit	http://meshlab.sourceforge.net	http://www.danielgm.net/cc	http://www.lancaster.ac.uk/staff/jamesm/software/sfm_georef.htm	http://ccwu.me/vsfm	http://sf3map.p.sic.es	https://photosynth.net	http://www.123dapp.com/catch
<i>Operative system</i>	Linux Windows	Linux Windows	Linux Mac Windows	Windows	Mac Windows	Linux Mac Windows	Windows	Linux Mac Windows	Windows	Windows	Windows Mac
<i>Camera calibration</i>			x								
<i>Bundle adjustment</i>	x			x				x	x	x	x
<i>Bundle adjustment with GCPs</i>			x								
<i>Sparse 3D reconstruction</i>	x		x	x				x	x	x	x
<i>Geo-referencing</i>			x				x	x	x		
<i>Dense 3D reconstruction</i>		x	x					x	x		x
<i>Post-processing</i>			x						x		
<i>Advanced cloud processing</i>					x	x					

1383 Table 3: Key developments of SfM photogrammetry towards a standard tool in
 1384 geomorphometry

1385
 1386

key developments	authors
method introduction	James & Robson (2012), Westoby et al. (2012), Fonstad et al. (2013)
evaluation of accuracy potential	James & Robson (2012), Westoby et al. (2012), Castillo et al. (2012)
SfM with terrestrial images	James & Robson (2012), Westoby et al. (2012), Castillo et al. (2012)
SfM with UAV images	Harwin & Lucieer (2012)
application with mm resolution	Bretar et al. (2013), Snapir et al. (2014)
application covering km ²	Immerzeel et al. (2014)
mitigation of systematic errors (i.e. dome)	James & Robson (2014a), Eltner & Schneider (2015)
influence of image network geometry	Micheletti et al. (2014), Piermattei et al. (2015)
usage of Smartphone for data acquisition	Micheletti et al. (2014)
time-lapse implementation	James & Robson (2014b)
influence of scale	Smith & Vericat (2015)
comparing tools	Stumpf et al. (2014), Eltner & Schneider (2015)
comparing cameras	Eltner & Schneider (2015), Prosdocimi et al. (2015)
synergetic usage of terrestrial and aerial images	Stöcker et al. (2015)
sub-merged topography	Woodget et al. (2015)
under water application	Leon et al. (2015)
multi-temporal application	James & Varley (2012), Lucieer et al. (2013)
reuse of historical images	Gomez et al. (2015)

1387

1388 Table 4. Overview of the publication history divided in the main topics from 2012 until
 1389 editorial deadline in Nov. 2015. Several publications examined more than one topic resulting
 1390 in a larger number of topics than actual publications (number in brackets in last row). IDs
 1391 refer to the table in appendix A1.

Topic	2012	2013	2014	2015	2016	ID	Total number of publications on the respective topic
Soil science/erosion	1	-	5	9	-	1, 2, 3, 5, 6, 9, 11, 18, 22, 23, 30, 31, 55, 60, 61	15
Volcanology	3	1	1	1	-	7, 15, 43, 44, 52, 54	6
Glaciology	-	-	4	6	-	12, 13, 14, 25, 27, 34, 37, 47, 51, 62	10
Mass movements	-	1	1	3	-	32, 35, 49, 56, 64	5
Fluvial morphology	-	1	5	3	1	4, 8, 16, 17, 21, 26, 29, 33, 37, 38	10
Coastal morphology	3	1	3	-	-	15, 20, 28, 36, 42, 50, 53	7
Others	1	2	8	5	-	7, 10, 17, 19, 24, 39, 40, 41, 45, 46, 48, 57, 58, 59, 63, 65	16
Topics (publications)	8 (6)	6 (6)	27 (25)	27 (27)	1(1)		69 (65)

1392
 1393
 1394
 1395
 1396

1397 Table 5: Data acquisition and error assessment protocol for SfM photogrammetry;
 1398 independent from individual study design.

<i>in the field:</i>					
target specifics	study area extent		ground control specifics	GCP measurement (total station, GPS, ...)	
	sensor to surface distance			GCP description	
	ground sampling distance			GCP number	
	target complexity			GCP accuracy	
camera specifics	camera name		image acquisition specifics	illumination condition	
	camera type (SLR, CSC, ...)			image number	
	lens type (zoom - fixed)			image overlap	
	sensor resolution			base (distance between images)	
	sensor size			network configuration (conv. - parallel-axis)	
	pixel size			perspective (aerial - terrestrial)	
	focal length		notes		
<i>at the office:</i>					
data processing specifics	SfM tool		accuracy assessment	registration residual	
	GCP integration (1-/2-staged)			reference type (LiDAR, RTK pts, ...)	
	output data type			reference error	
error ratios	relative error			error measure (M3C2, raster difference, ...)	
	reference superiority		statistical value (RMSE, std dev, ...)		
	theoretical error ratio		notes		

1400 Figure captions

1401

1402 Figure 1: Schematic illustration of the versatility of SfM photogrammetry.

1403

1404 Figure 2. Map of the research sites of all studies of this review.

1405

1406 Figure 3. Variety of SfM photogrammetry tools used in the 65 reviewed studies.

1407

1408 Figure 4. Boxplots summarizing statistics: a) of the scale of the study reaches (N: 56; ID 1-3
1409 and 5-39 in Appendix A), b) the relative error (calculated in regard to distance and measured
1410 error, N: 54; ID 1-3, 5-12 and 14-39 in Appendix A), and c) the reference superiority
1411 (calculated in regard to measured error and reference error, N: 33; ID 1-30 and 32-39 in
1412 Appendix A) of reviewed studies.

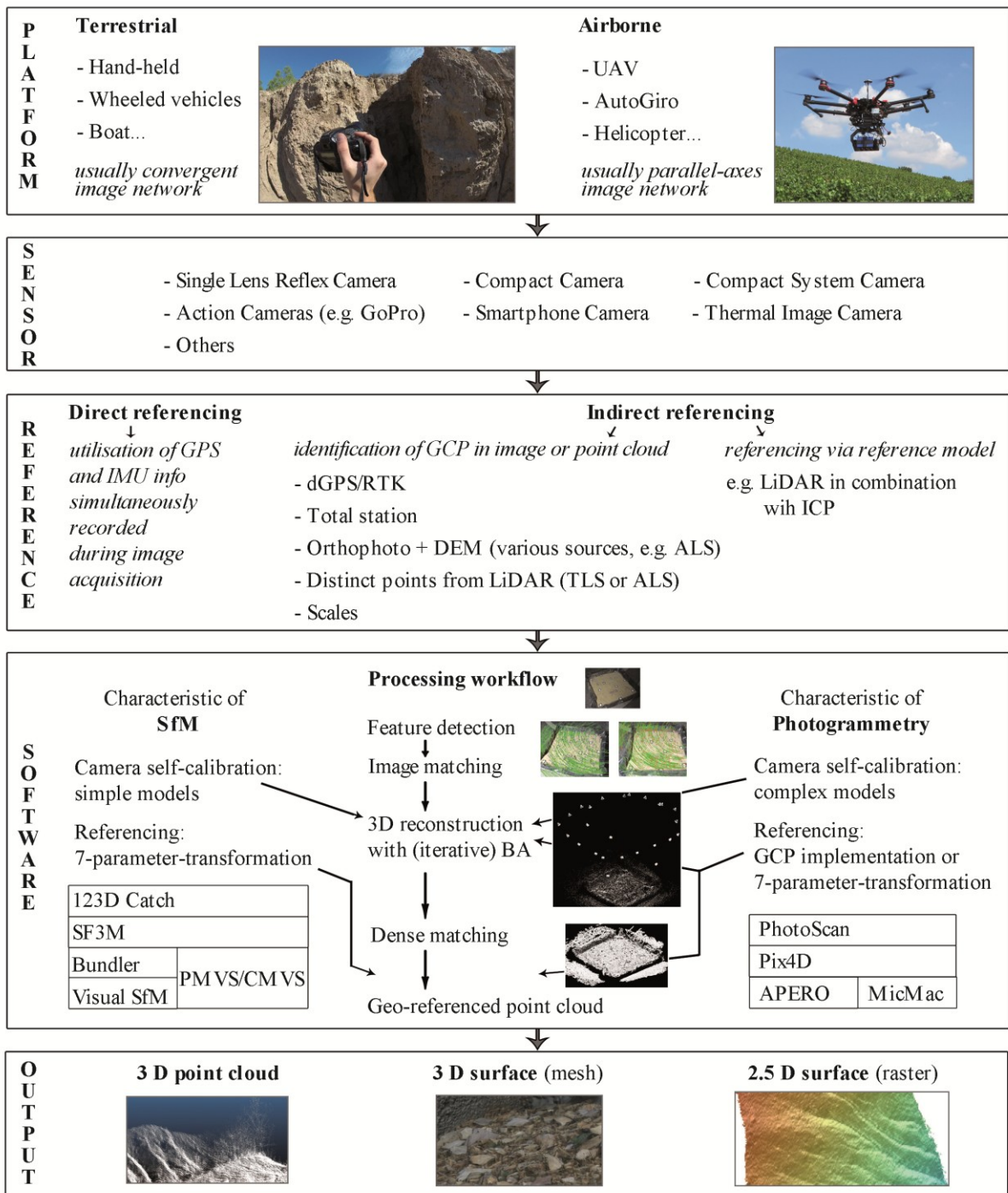
1413

1414 Figure 5. Performance of several error parameters in regard to the camera to surface
1415 distance. a) Characteristics of measured error and relative error (N: 54; ID 1-3, 5-12 and 14-39
1416 in Appendix A) . For grey coloured points GCPs are measured in point cloud (in total 9 times
1417 corresponding to the studies: ID 8, 11, 12, 28, 36, 37 in Appendix A) and for white points
1418 GCPs are measured in images (corresponding to the remaining studies) for model
1419 transformation. b) Superiority of the reference data (N: 33), which is calculated as ratio
1420 between measured error and error of the reference. Area based (ID 5-7, 12, 15, 17, 22, 25, 26,
1421 30 and 32 in Appendix A) and point based (ID 2, 3, 8, 9, 20, 24, 28-30, 33, 35 and 37 in
1422 Appendix A) reference measurements are distinguished. c) Theoretical error ratio, considering
1423 the theoretical and measured error, to illustrate SfM photogrammetry performance in field
1424 applications (N: 23; ID 1-3, 8, 10-12, 15, 21, 22, 25, 26, 28-30 and 32 in Appendix A).

1425

1426

1427 Figure 1:



1428

1429

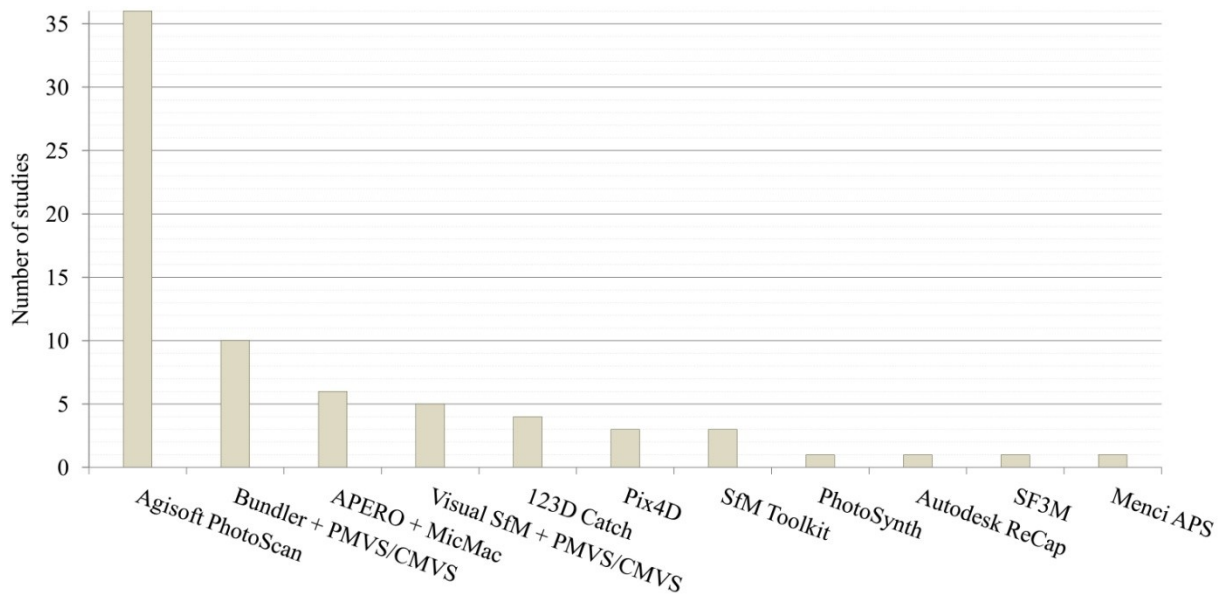
1430 Figure 2:



1431

1432

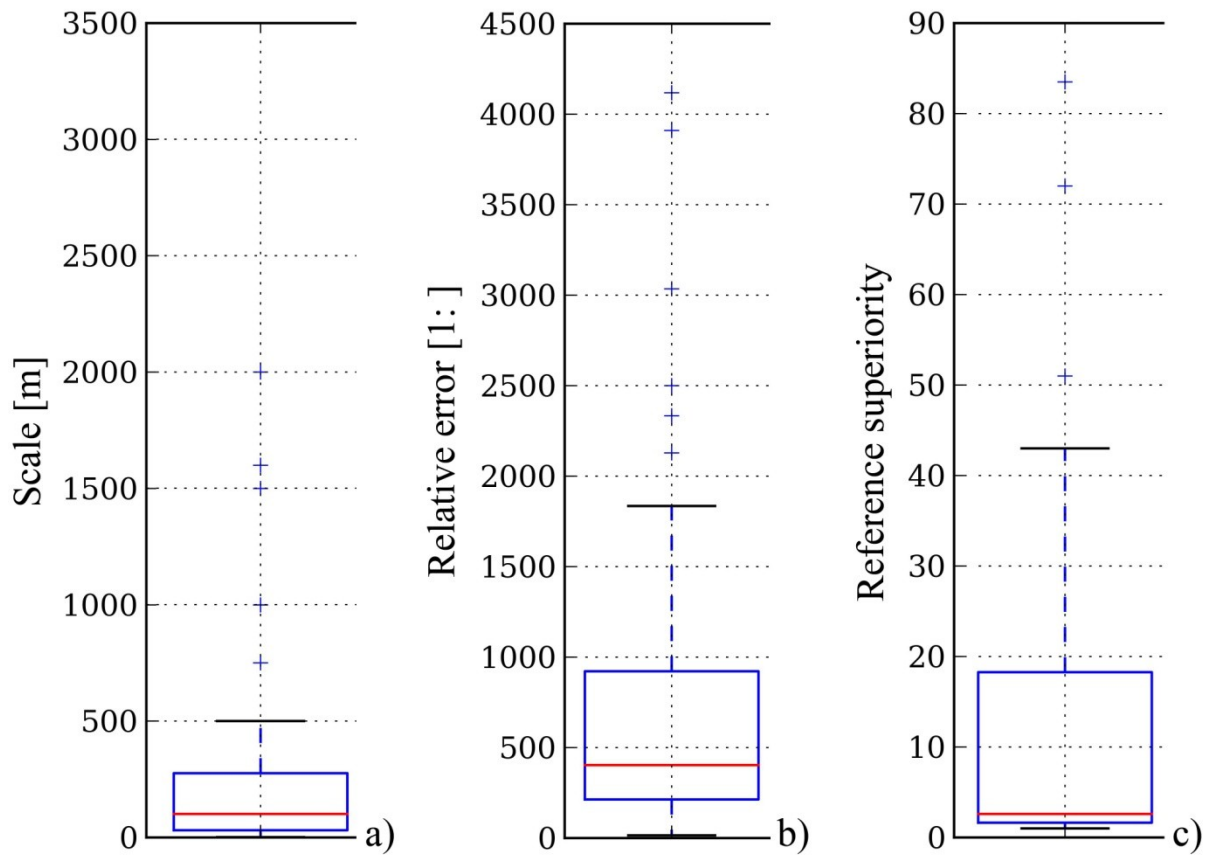
1433 Figure 3:



1434

1435

1436 Figure 4:



1437

1438

